ARTICLE

# A mutation in *SLC37A4* causes a dominantly inherited congenital disorder of glycosylation characterized by liver dysfunction

Bobby G. Ng,[1,23] Paulina Sosicka,[1,23] François Fenaille,[2] Annie Harroche,[3] Sandrine Vuillaumier-Barrot,[4,5] Mindy Porterfield,[6] Zhi-Jie Xia,[1] Shannon Wagner,[6] Michael J. Bamshad,[7,8] Marie-Christine Vergnes-Boiteux,[9] Sophie Cholet,[2] Stephen Dalton,[10,11] Anne Dell,[12] Thierry Dupré,[4] Mathieu Fiore,[9,13] Stuart M. Haslam,[12] Yohann Huguenin,[14] Tadahiro Kumagai,[6] Michael Kulik,[10,11] Katherine McGoogan,[15] Caroline Michot,[16] Deborah A. Nickerson,[8] Tiffany Pascreau,[17] Delphine Borgel,[17,18] Kimiyo Raymond,[19] Deepti Warad,[20] University of Washington Center for Mendelian Genomics (UW-CMG), Heather Flanagan-Steet,[21] Richard Steet,[21] Michael Tiemeyer,[6] Nathalie Seta,[4] Arnaud Bruneel,[4,22] and Hudson H. Freeze[1,*]

## Summary

*SLC37A4* encodes an endoplasmic reticulum (ER)-localized multitransmembrane protein required for transporting glucose-6-phosphate (Glc-6P) into the ER. Once transported into the ER, Glc-6P is subsequently hydrolyzed by tissue-specific phosphatases to glucose and inorganic phosphate during times of glucose depletion. Pathogenic variants in *SLC37A4* cause an established recessive disorder known as glycogen storage disorder 1b characterized by liver and kidney dysfunction with neutropenia. We report seven individuals who presented with liver dysfunction multifactorial coagulation deficiency and cardiac issues and were heterozygous for the same variant, c.1267C>T (p.Arg423*), in *SLC37A4*; the affected individuals were from four unrelated families. Serum samples from affected individuals showed profound accumulation of both high mannose and hybrid type N-glycans, while N-glycans in fibroblasts and undifferentiated iPSC were normal. Due to the liver-specific nature of this disorder, we generated a CRISPR base-edited hepatoma cell line harboring the c.1267C>T (p.Arg423*) variant. These cells replicated the secreted abnormalities seen in serum N-glycosylation, and a portion of the mutant protein appears to relocate to a distinct, non-Golgi compartment, possibly ER exit sites. These cells also show a gene dosage-dependent alteration in the Golgi morphology and reduced intraluminal pH that may account for the altered glycosylation. In summary, we identify a recurrent mutation in *SLC37A4* that causes a dominantly inherited congenital disorder of glycosylation characterized by coagulopathy and liver dysfunction with abnormal serum N-glycans.

## Introduction

Congenital disorders of glycosylation (CDGs) are a clinically and biochemically heterogenous group of disorders characterized by abnormal lipid or protein glycosylation.[1,2] To date, more than 140 types of CDGs have been identified across at least seven different glycosylation pathways.[2] The vast majority of CDGs follow an autosomal recessive or X-linked inheritance pattern, although disorders due to *de novo* or dominant variants have been observed with increased frequency.[3] In several instances, a single gene has been shown to cause both dominantly and recessively inherited disorders that present with unique phenotypes as is the case for *DHDDS* (MIM: 608172), *NUS1* (MIM: 610463), *POFUT1* (MIM: 607491), and *COG4* (MIM: 606976).[4–8]

*SLC37A4* (MIM: 602671) encodes for a multitransmembrane domain glucose-6-phosphate (Glc-6P) transporter that is localized to the endoplasmic reticulum (ER).[9,10] In gluconeogenic organs, such as the liver and kidney, its primary function is to transport Glc-6P into the ER during times of glucose depletion, thus regulating

[1]Human Genetics Program, Sanford Burnham Prebys Medical Discovery Institute, La Jolla, CA 92037, USA; [2]Université Paris-Saclay, CEA, INRAE, Département Médicaments et Technologies pour la Santé, MetaboHUB, 91191 Gif sur Yvette, France; [3]Hôpital Necker, Haemophilia Care Centre, 75015 Paris, France; [4]AP-HP, Hôpital Bichat-Claude Bernard, Biochimie Métabolique et Cellulaire, 75018 Paris, France; [5]INSERM U1149, Université de Paris, 75018 Paris, France; [6]Complex Carbohydrate Research Center, Department of Biochemistry and Molecular Biology, University of Georgia, Athens, GA 30602, USA; [7]Department of Pediatrics, University of Washington, Seattle, WA 98195, USA; [8]Department of Genome Sciences, University of Washington, Seattle, WA 98195, USA; [9]Laboratoire d'Hématologie, CHU de Bordeaux, 33604 Pessac, France; [10]Center for Molecular Medicine, University of Georgia, Athens, GA 30602, USA; [11]Department of Biochemistry and Molecular Biology, University of Georgia, Athens, GA 30602, USA; [12]Department of Life Sciences, Imperial College London, SW7 2AZ London, UK; [13]Centre de Référence des Pathologies Plaquettaires Constitutionnelles, CHU de Bordeaux, 33604 Pessac, France; [14]Centre de Ressources et de Compétence des Maladies Hémorragiques Constitutionnelles, CHU de Bordeaux, 33076 Bordeaux, France; [15]Medical Director of Hepatology Nemours Children's Specialty Care, Jacksonville, FL 32207, USA; [16]Department of Clinical Genetics and Reference Centre for Constitutional Bone Diseases, INSERM U1163, Université de Paris, Imagine Institute, Necker-Enfants Malades Hospital, AP-HP, 75015, Paris, France; [17]Laboratoire d'Hématologie Biologique, AP-HP, Hôpital Necker Enfants Malades, 75015 Paris, France; [18]HITh, UMR_S 1176, INSERM, Université Paris-Saclay, 94270 Le Kremlin-Bicêtre, France; [19]Biochemical Genetics Laboratory, Mayo Clinic College of Medicine, Rochester, MN 55905, USA; [20]Division of Pediatric Hematology Oncology, Mayo Clinic, Rochester, MN 55905, USA; [21]JC Self Research Institute, Greenwood Genetic Center, Greenwood, SC 29646, USA; [22]INSERM UMR1193, Université Paris-Saclay, 92290 Châtenay-Malabry, France
[23]These authors contributed equally
*Correspondence: hudson@sbpdiscovery.org
https://doi.org/10.1016/j.ajhg.2021.04.013.

glucose homeostasis.[10] SLC37A4 does this in cooperation with various tissue-specific phosphatases (G6PC, G6PC2, and G6PC3) to hydrolyze Glc-6P to glucose and inorganic phosphate (Pi), which exit the ER. Glucose is subsequently transported out of the cell to maintain glucose homeostasis.[10,11] SLC37A4 also participates in the ER-localized pentose phosphate pathway (PPP) by providing Glc-6P to hexose-6-phosphate dehydrogenase (H6PD), which catalyzes the first two reactions of ER-localized PPP generating nicotinamide adenine dinucleotide phosphate (NADPH).[12]

Pathogenic variants in *SLC37A4* cause autosomal recessive glycogen storage disorder 1b (GSD1b) (MIM: 232220), which is characterized by an inability to properly metabolize glycogen.[9,13] This results in the accumulation of glycogen in gluconeogenic organs such as the liver and kidneys, ultimately leading to organ dysfunction and disease.[9,13] Neutropenia is frequently seen in affected individuals as well. Pathogenic variants in the tissue-specific phosphatases have also been identified. GSD1a (also known as von Gierke disease) (MIM: 232200) is caused by mutations in *G6PC* (MIM: 613742), causing similar accumulation of glycogen in the liver and kidney.[14,15] Pathogenic variants in *G6PC3* (MIM: 611045) cause autosomal recessive severe congenital Neutropenia 4 and Dursun syndrome (MIM: 612541).[16,17] Cortisone reductase deficiency 1 (MIM: 604931) is caused by pathogenic variants in *H6PD* (MIM: 138090).[18]

We report the molecular, biochemical, and clinical characterization of seven individuals who clinically presented with a coagulopathy affecting several coagulation factors and were heterozygous for a c.1267C>T (p.Arg423*) variant in *SLC37A4*; the affected individuals were from four unrelated families. All affected individuals were identified by coagulation abnormalities and subsequently found to have abnormal N-glycosylation of serum glycoproteins, specifically the accumulation of high mannose and hybrid type N-glycans. Introduction of the c.1267C>T (p.Arg423*) variant into Huh7 hepatocellular carcinoma cells revealed clear gene dosage-dependent morphological and functional deficiencies in the Golgi apparatus function that recapitulate the abnormal N-glycans seen in our affected individuals.

## Material and methods

### Subjects

Families included in our SLC37A4-CDG research study provided written consent under an approved Sanford Burnham Prebys Medical Discovery Institute IRB protocol or an approved IRB through each family's primary medical physician. The only inclusion criteria for this study was the presence of the c.1267C>T (p.Arg423*) variant in *SLC37A4*. Blood samples were obtained for all individuals. Primary fibroblasts were obtained for two affected individuals (P6 and P7) and grown from a skin biopsy obtained by the subjects' physician.

### Genomic analysis

Exome sequencing (ES) and genome sequencing (GS) with analysis were carried out by two independent groups with a shared heterozygous c.1267C>T (p.Arg423*) variant in *SLC37A4* identified in all affected individuals. Sanger sequencing of all seven affected individuals and unaffected family members was used to confirm presence of the variant and to assess segregation. Primers to amplify exon 10 of *SLC37A4* are available upon request.

### Cell culture

Fibroblasts from apparently healthy controls GM-00038, GM-05565, and GM-09503 (Coriell Institute); proband primary fibroblasts (P6 and P7); and the hepatocellular carcinoma line Huh7 were grown (unless otherwise stated) in complete 1 g/L (5.5 mM) glucose containing Dulbecco's modified Eagle's medium (Corning) supplemented with 10% heat-inactivated fetal bovine serum (Sigma-Aldrich LOT# H176268), 100 U/mL penicillin and 100 mg/mL streptomycin (GIBCO), and 2 mM L-Glutamine (GIBCO). Induced pluripotent stem cells (iPSCs) were established from affected individual fibroblasts as described previously.[19] The wild-type control iPSC line K3 was utilized.[20] Human iPSCs were generated via lentivirus transduction of pluripotency factors as described previously.[21] Human hepatocytes from individual P7-derived cells were generated by a previously reported method.[19]

### Glycosylation studies

Individuals P1, P2, P4, P5, and P6, all had carbohydrate-deficient transferrin (CDT) analysis performed with capillary zone electrophoresis (CZE), while P7 had both electrospray ionization mass spectrometry (ESI-MS) and liquid chromatography-mass spectrometry (LC-MS) as previously described.[22–24] Apolipoprotein C-III (apoC-III) mucin core 1 O-glycosylation was analyzed with 2D electrophoresis as previously described.[25] Profiles of total serum N-glycans were obtained by matrix-assisted laser desorption/ionization time-of-flight mass spectrometry (MALDI-TOF MS) following N-glycan cleavage by peptide N-glycosidase F (PNGase F) and permethylation as previously described.[26] Analysis of iPSCs, derived hepatocytes, and Huh7-edited cell line-secreted and cell-associated N-glycans was performed by multi-dimensional nanospray ionization mass spectrometry (NSI-MSn) as previously described.[27] High performance liquid chromatography (HPLC) analysis of N-glycans secreted by CRISPR-edited Huh7 cells was done following labeling with procainamide (ProA) reagent as described with modification available upon request.[28]

### CRISPR-edited Huh7 cell line

The guide RNA (gRNA) sequencing GATGGGCCGAGTGTCCAAGA targeting exon 10 of *SLC37A4* was cloned into pGuide-EF1a-GFP (OriGene - GE100044). This vector does not express Cas9, only the gRNA to *SLC37A4* and turboGFP (tGFP), which allows for sorting positively transfected cells. Both pGuide-R423X-SLC37A4 and pCMV-BE3 (Addgene plasmid 73021) were co-transfected together into Huh7 cells and allowed to grow for 48 h. Subsequently, tGFP positive cells were fluorescence-activated cell sorting (FACS) sorted with a FACSAria IIu instrument (BD Biosciences) into 96-well plates to generate isogenic clones, which were expanded and screened by Sanger sequencing.

### Cellular fractionations

Subcellular fractionations were performed as previously described with some modifications.[29,30] Briefly, cells from one 150 mm plate were washed twice with Dulbecco's phosphate-buffered saline (DPBS) and then homogenized in buffer (10 mM HEPES-KOH, 25 mM KCl, 250 mM sucrose, and 1 mM EDTA, pH 7.4, protease

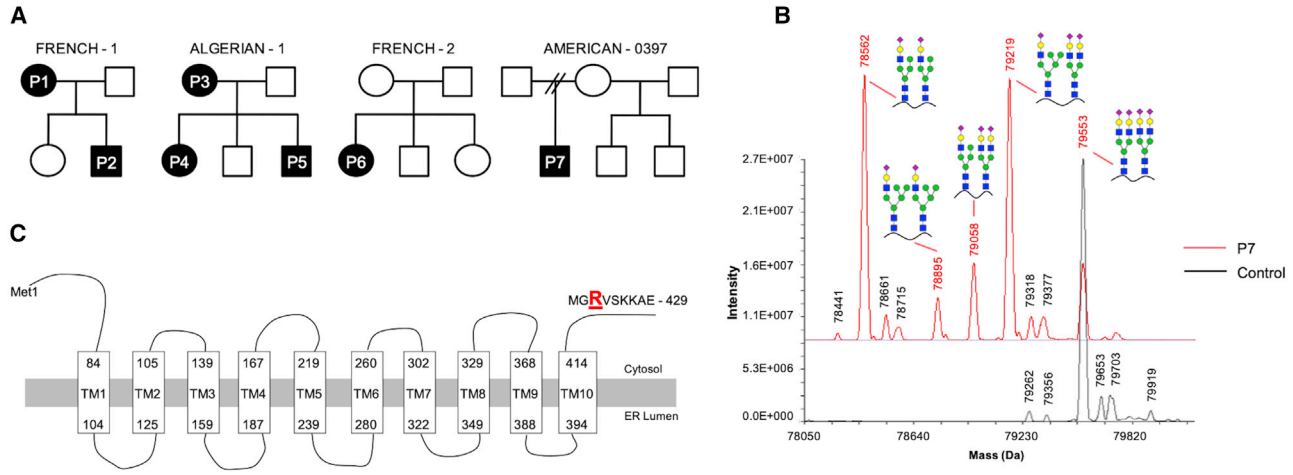


**Figure 1. Identification of a recurrent *SLC37A4* mutation in four unrelated families**
(A) Pedigrees showing segregation of the *SLC37A4* c.1267C>T (p.Arg423*) mutation in seven affected individuals from four unrelated families.
(B) LC-MS of serum transferrin from control and P7 serum with deconvoluted masses of intact serum TF from full scans showing the appearance of several peaks corresponding to distinctive peaks containing hybrid N-glycans.
(C) Schematic of human SLC37A4 showing the p.Arg423* localizing to the cytoplasmic tail (UniProt: O43826-1).

inhibitor cocktail [Thermo Fisher Scientific]) by passing through 27-gauge needle 15 times. A post-nuclear supernatant (PNS) was separated by centrifugation at 1,000*g* for 15 min at 4°C and then subjected to 15,000*g* spin for 20 min at 4°C. The resulting pellet was resuspended in 5% Nycodenz, applied to a 10%–24% discontinuous Nycodenz gradient (Fisher Scientific), and centrifuged at 100,000*g* in an SW40 rotor for 18 h at 4°C. Fractions (1 mL) were collected, trichloroacetic acid (TCA) precipitated, dissolved in 2× loading buffer, and analyzed by SDS-PAGE.

### Immunofluorescence

Cells were seeded on Millicell EZ 8-well glass slides (Sigma Aldrich) and, 1 day later, washed twice with DPBS and fixed for 15 min with 4% PFA at room temperature. Next, cells were washed three times with DPBS and blocked with 1% BSA solution in DPBS containing 0.1% saponin. After 1 h of blocking at room temperature, respective primary antibodies (Table S1), diluted in blocking solution, were added and slides were incubated overnight at 4°C. The next day, cells were washed three times with blocking solution and respective secondary antibodies (Table S1) diluted in blocking solution. After 1-h incubation at room temperature, DAPI (Thermo Fisher Scientific) was added directly to the solution, so its final dilution was 1:500. 20 min later, cells were washed twice with blocking buffer, twice with DPBS, and twice with water. Cover slides were stuck to the slides via Immu-Mount mounting medium (Thermo Fisher Scientific). Cells were analyzed with LSM 710 Zeiss confocal microscope and EC Plan-Neofluar 40×/1.30 Oil DIC M27 objective. For immunostaining of iPSC-derived hepatocytes, differentiated hepatocyte spheroids were seeded in Matrigel-coated slide chambers and grown for 48 h to allow a monolayer of cells to migrate from the spheroid prior to fixation and staining as described above.

### Golgi pH measurements

Golgi pH measurements were performed as described by Galenkamp et al.[31] Briefly, Huh7 or fibroblast cells were seeded on 6-well plates and, after 24 h, transfected with GalT-mCherry-eGFP construct via FuGENE HD (Promega) according to the manufacturer's instructions. 24 h after transfection, cells were seeded on CELLview glass bottom cell culture dishes (Greiner Bio-One). 48 h later, cells were washed twice with DPBS and media exchanged for phenol red-free DMEM 4.5 g/L glucose media (Thermo Fisher Scientific). For pH determinations, cells were incubated for 15 min with one of the calibration buffers: 30 mM ammonium formate (pH 4.9), 30 mM 2-Morpholinoethanesulfonic acid (MES) (pH 5.4), 30 mM MES (pH 5.9), 30 mM 3-(N-morpholino)propanesulfonic acid (MOPS) (pH 6.5), 30 mM MOPS (pH 7.0), supplemented with 130 mM KCl, 1 mM $MgCl_2$, 10 μM Nigericin, 10 μM Valinomycin, and 10 μM Monensin. Imaging was performed on living cells at room temperature and at atmospheric $CO_2$ via Zeiss LSM 710 laser scanning confocal microscope and C-Apochromat 40×/1.20 W Korr FCS M27 water immersion objective. eGFP and mCherry signals were collected simultaneously by 488 nm and 594 nm excitation and ratios were determined by region of interest selection of fluorescence via ImageJ software (NIH).

### Transport assay

SLC37A4 transport assays were performed as previously described.[13]

## Results

### Clinical summary for seven individuals presenting with liver dysfunction

A cohort of seven individuals, from four unrelated non-consanguineous families, with an undefined type II CDG (Figure 1A) were found to have a strikingly similar clinical phenotype involving liver dysfunction with abnormal coagulation factor activities. All individuals had an abnormal CDT and apolipoprotein C-III (apoC-III) pattern.

P1 is a 35-year-old female of French origin with a history of elevated aspartate aminotransferase (AST) level (91 U/L; normal value < 35 U/L) but normal alanine aminotransferase (ALT) on routine blood analysis. A complete blood

**Table 1. Clinical summary of seven individuals carrying the c.1267C>T (p.Arg423*) variant in *SLC37A4***

| | P1 | P2 | P3 | P4 | P5 | P6 | P7 | Marquardt et al.[32] | Wilson et al.[33] | Current cohort summary |
|---|---|---|---|---|---|---|---|---|---|---|
| Family | French-1 | French-1 | Algerian-1 | Algerian-1 | Algerian-1 | French-2 | American-0397 | – | – | – |
| Gender | female | male | female | Female | male | female | male | female | female | – |
| Year of birth | 1985 | 2018 | 1973 | 2002 | 2007 | 2010 | 2009 | N/A | 1997 | – |
| Age of diagnosis | 29 years | 1 month | 42 years | 11 years | 4 months | 8 years | 5 years | 10 weeks | 36 days | – |
| Variant | c.1267C>T (p.Arg423*) | c.1267C>T (p.Arg423*) | c.1267C>T (p.Arg423*) | c.1267C>T (p.Arg423*) | c.1267C>T (p.Arg423*) | c.1267C>T (p.Arg423*) | c.1267C>T (p.Arg423*) | c.1267C>T (p.Arg423*) | c.1267C>T (p.Arg423*) | – |
| Inheritance | unknown | maternally inherited | unknown | maternally inherited | maternally inherited | *de novo* | *de novo* | *de novo* | *de novo* | – |
| Method of detection | ES | Sanger | ES | ES | ES | Sanger | ES/GS | ES | ES | – |
| CDT results | abnormal-type II | abnormal-type II | abnormal-type II | abnormal-type II | abnormal-type II | abnormal-type II | abnormal-type II | abnormal-type II | abnormal-type II | 7/7 |
| apoC-III | altered O-glycan | altered O-glycan | altered O-glycan | altered O-glycan | altered O-glycan | altered O-glycan | altered O-glycan | N/A | N/A | 7/7 |
| Serum N-glycans | high man, hybrid | high man, hybrid | high man, hybrid | high man, hybrid | high man, hybrid | high man, hybrid | high man, hybrid | high man, hybrid | high man, hybrid | 7/7 |
| Cardiac abnormalities | none reported | perimembranous ventricular septal defect | none reported | none reported | tetralogy of Fallot | ventricular septal defect | none reported | none reported | none reported | 3/7 |
| Skeletal abnormalities | no | no | scoliosis | scoliosis | kyphoscoliosis | no | no | no | scoliosis | 3/7 |
| Ankyloglossia | no | no | no | no | yes | no | no | yes | no | 1/7 |
| AST (ref. 7–40 U/L) | 65 U/L (H) | N/A | 50 U/L (H) | 77 U/L (H) | 91 U/L (H) | 147 U/L (H) | 80 U/L (H) | 228 U/L (H) | 522 U/L (H) | 6/6 |
| F2 (ref. 60%–140%) | 31 (L) | 22 (L) | 57 (L) | 30 (L) | 20 (L) | 18 (L) | 27 (L) | 5.5 (L) | N/A | 7/7 |
| F5 (ref. 60%–140%) | 51 (L) | 52 (L) | 64 | 40 (L) | 39 (L) | 50 (L) | 29 (L) | 38.5 (L) | N/A | 6/7 |
| Fg (ref. 1.5–3.5 g/L) | 1.7 g/L | 1.7 g/L | 2.8 g/L | 1.8 g/L | 1.3 g/L (L) | 1.7 g/L | 1.5 g/L | 0.4 g/L (L) | 0.1 g/L (L) | 1/7 |
| F8 (ref. 60%–150%) | 117 | N/A | 165 | 130 | 144 | 109 | 85 | N/A | N/A | 0/6 |
| F9 (ref. 60%–140%) | 63 | N/A | 85 | 58 (L) | 42 (L) | 55 (L) | 44 (L) | N/A | N/A | 4/6 |
| F11 (ref. 60%–140%) | 59 (L) | N/A | 55 (L) | 31 (L) | 34 (L) | 22 (L) | 33 (L) | N/A | normal | 6/6 |
| SERPINC1 (ref. 80%–120%) | 28 (L) | 34 (L) | 60 (L) | 37 (L) | 32 (L) | 19 (L) | 32 (L) | 0 (L) | normal | 7/7 |
| PROC (ref. 50%–120%) | 110 | 49 | 97 | 72 | 73 | 59 | 94 | N/A | normal | 0/7 |
| PROS1 (ref. 60%–120%) | 41 (L) | 48 (L) | 70 | 43 (L) | 81 | 35 (L) | 35 (L) | N/A | normal | 5/7 |

Reference ranges: ALT, ref.; AST, ref. 7–40 U/L; F2, ref. 60%–140% activity; F5, ref. 60%–140% activity; Fg (g/L), ref. 1.5–3.5 g/L; F8, ref. 60%–150% activity; F9, ref. 60%–140% activity; F11, ref. 60%–140% activity; SERPINC1, ref. 80%–120% activity; PROC, ref. 50%–120% activity; PROS1, ref. 60%–120% activity. Abbreviations are as follows: L, low; H, high; N/A, not available.

count, as well as prothrombin time (PT) and activated partial thromboplastin time (aPTT), was normal. However, clotting factor II (F2) was unexpectedly decreased (42%), while factor V (F5), factor VII (F7), factor VIII (F8), factor IX (F9), factor X (F10), factor XI (F11), factor XII (F12), and fibrinogen (Fg) were within a normal range (Table 1). Medically assisted reproduction led to a non-hemorrhagic spontaneous abortion followed by two successful

pregnancies. During this 4-year period, antithrombin (SERPINC1) and F2 levels were often markedly decreased (SERPINC1, 23% to 52%, mean: 45%; F2, 29% to 67%, mean: 38%) with low levels of protein S (PROS1) (45% to 53%). AST levels were consistently elevated (62 U/L to 91 U/L, mean: 73 U/L) (Table 1). The unexplained fluctuating coagulation abnormalities seen in P1 led to CDG screening, which showed a marked CDG-II transferrin CDT pattern coupled with altered apoC-III glycoforms (Table 1; Figures S1 and S2).

P2 is the second child of P1 (Figure 1A). At around 1 month of age, his pre-surgical testing for perimembranous ventricular septal defects (VSDs) showed similar coagulation abnormalities and CDT pattern as his mother. No bleeding episodes occurred during this corrective surgery. At 6 months of age, his coagulation parameters were globally altered with F2 (22%), F5 (52%), PROS1 (48%), SERPINC1 (34%), and protein C (PROC) (49%) (Table 1), however, there were no bleeding or thrombotic episodes. He, like his mother, also showed the same CDG-II CDT and altered apoC-III glycoform profile (Table 1; Figures S1 and S2).

P3 is an adult female of Algerian origin (Figure 1A). At 42 years of age, moderate deficiencies in both clotting factors and coagulation inhibitors were noted, including F2 (57%), F11 (55%), and SERPINC1 (60%), with normal PT, aPTT, Fg, PROC, and PROS1 (Table 1). She had neither bleeding nor thrombotic symptomatology. Besides progressive deafness, strabismus treated by surgery, and delayed diagnosed scoliosis, she had a normal clinical examination. Complete blood count was normal, but an elevated AST (50 U/L) was noted (Table 1). CDT and apoC-III analyses were unable to be performed for P3.

P4 is a female and the first child of P3 (Figure 1A). P4 has had multiple operations under fresh frozen plasma (FFP) and tranexamic acid for repair of a severe lip/palate cleft with bifid uvula. At 13 years of age, she showed altered PT (56%) and aPTT ratio (1.49) with normal F8 and F9. An overall decrease was seen in both the procoagulant factors F2 (30%) and F5 (40%) and anticoagulant factors SERPINC1 (37%) and PROS1 (43%) (Table 1). A complete blood count was normal, as were liver ALT and bilirubin levels. However, AST was elevated (77 U/L) (Table 1). CDG screening tests showed the same CDG II CDT pattern and abnormal apoC-III patterns (Table 1; Figures S1 and S2).

P5 is a male sibling of P4 and the third child of P3 (Figure 1A). At 4 months of age, PT and aPTT ratios were 61% and 1.72, respectively, with markedly decreased F2 (20%) and F11 (30%) with normal F5, Fg, F8, and F9 (Table 1). 1 month later, examination showed decreased SERPINC1 (32%) but normal PROC and PROS1. P5 had a tetralogy of Fallot surgically repaired at the age of 6 months, and at 2 years of age, he had a tongue-tie surgery (under FFP), both without complications. At 5 and 8 years of age, coagulation defects were seen in F2 (17% and 20%) and F5 (41% and 39%). At 8 years of age, AST level was elevated (91 U/L) with normal ALT (Table 1). There was a tendency for easily bruising (in contrast with his sister P4) and he had impaired wound healing. However, no bleeding disorders were reported. CDG screening tests showed a CDG II CDT and abnormal apoC-III pattern (Table 1; Figures S1 and S2).

P6 is a female of French origin (Figure 1A) who, at 8 years of age, showed a coagulation profile with altered PT (62%) and aPTT (ratio 1.86) with markedly decreased activities of F2 (18%) and F11 (22%) and decreased F5 (50%), F7 (44%), and F10 (48%). Coagulation inhibitors SERPINC1 and PROS1 were markedly decreased (19% and 35%) with normal PROC (Table 1). A complete blood count was normal, and no bleeding disorders were reported. She has a VSD under clinical supervision. A vesicoureteral reflux and strabismus were noted. Apparently healthy parents and two younger siblings had normal CDT patterns, while P6 had the same abnormal CDG II CDT and apoC-III patterns (Table 1; Figure S1 and S2).

P7 is a male of Irish-American origin (Figure 1A), born to healthy non-consanguineous parents, who displayed a long history of easy bruising and bleeding. Prior to a tonsillectomy and adenoidectomy, coagulation test revealed abnormalities in multiple coagulation factors, including F2 (27%), F5 (29%), F11 (37%), and PROS1 (35%). Liver function tests showed elevated liver enzyme AST (80 U/L) (Table 1). A liver biopsy determined no fibrosis or gross abnormalities. However, due to the history of elevated AST and abnormal coagulation factors, CDT screening was performed with both LC-MS and ESI-MS that showed accumulation of multiple high mannose and/or hybrid type N-glycans (Figure 1B; Table 1). An abnormal apoC-III pattern was also seen for P7 (data not shown).

In total, from our cohort, 7/7 (100%) individuals showed decreases in both F2 and SERPINC1 activities, 6/7 (86%) showed reduced F5 activity, 6/6 (100%) reduced F11 activity, 5/7 (71%) reduced protein S, and 4/6 (67%) reduced F9. AST levels were elevated in 6/6 (100%) individuals tested, while ALT was unaffected in all. (Table 1). F8 was within the reference range for all seven individuals, most likely because it is produced by non-hepatocyte endothelial cells. No neurological deficiencies were noted in the seven individuals. For all seven affected individuals, no candidate gene was identified through either clinical or glycan phenotyping. Recently, two more individuals were reported to carry the c.1267C>T (p.Arg423*) variant in *SLC37A4* and presented with strikingly similar biochemical and clinical phenotypes (Table 1).[32,33] A less frequently shared feature included ankyloglossia, which was treated in both affected individuals (Table 1).

### Glycosylation studies of serum showing accumulation of high mannose and hybrid type N-glycans

P1, P2, P4, P5, and P6 showed abnormalities consistent with a type II CDG by CZE (Figure S1). In P7, LC-MS showed the accumulation of several glycans absent from control samples. On the basis of the assigned masses for each of these peaks, we predicted they represented

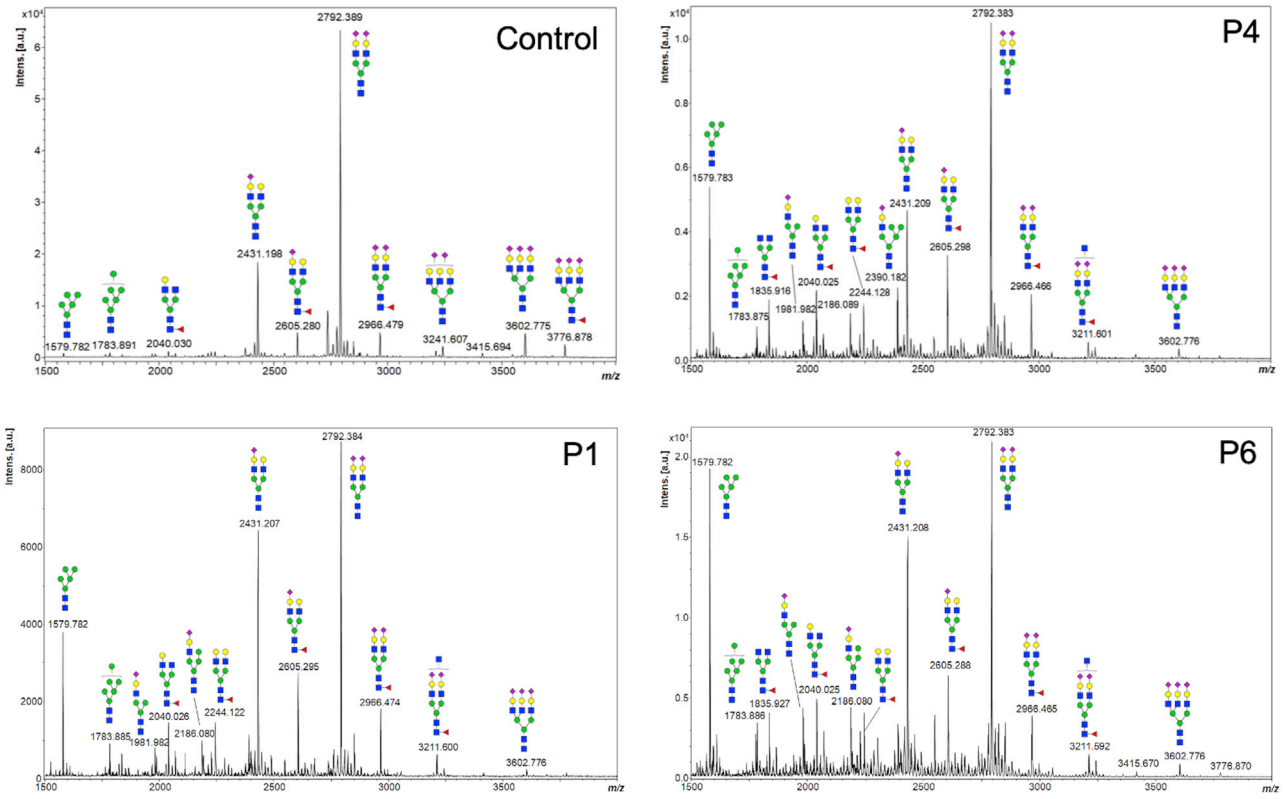


**Figure 2. N-glycan abnormalities in serum from affected individuals**
MALDI-TOF MS spectra of serum protein-derived N-glycans from unrelated individuals (P1, P4, and P6) are abnormal. Specifically, both high mannose (peaks at *m/z* 1,579.8 and 1,783.9) and hybrid type N-glycans (peaks at *m/z* 1,981.9, 2,186.1, and 2,390.2) increases were seen in positive-ion mode as sodiated forms. Green circles, mannose; yellow circles, galactose; blue squares, N-acetyl glucosamine; red triangles, fucose; purple diamonds, sialic acid.

transferrin (TF) containing high mannose and/or hybrid type N-glycans (Figure 1B).

We used MALDI-TOF MS to analyze N-glycans from total serum glycoproteins and found that all seven individuals accumulated multiple species of both oligo and high mannose (e.g., peaks at *m/z* 1,579.8 and 1,783.9) and hybrid type N-glycans (e.g., peaks at *m/z* 1,981.9, 2,186.1, and 2,390.2) (Figures 2 and S3). These changes suggested alterations in the *cis* and medial Golgi compartments. Accumulation of truncated N-glycans with deficiencies in galactosylation (e.g., peaks at *m/z* 1,835.9 and 2,040.0) were also observed and suggests a defect in the *trans*-Golgi compartment (Figures 2 and S3).

A similar N-glycan phenotype occurs in cell lines defective in Golgi α-Mannosidase II (MAN2A1) or cells treated with the α-mannosidase II inhibitor swainsonine.[34] On the basis of this similarity, individual P7 was Sanger sequenced for the entire coding, intronic, and promotor regions of both *MAN2A1* (MIM: 154582) and its paralog *MAN2A2* (MIM: 600988). However, no likely pathogenic variants were identified in either gene.

### Identification of a recurrent c.1267C>T (p.Arg423*) variant in *SLC37A4*

ES was performed on individuals P1, P3, P4, and P5. ES and GS were performed on P7. Sanger sequencing was used for P2 and P6. All seven individuals were found to share a heterozygous and likely pathogenic variant c.1267C>T (p.Arg423*) in *SLC37A4* (Table 1; Figure 1C). The variant in P6 and P7 was found to be *de novo*, while it was maternally inherited for P2, P4, and P5 (Table 1). Inheritance is unclear for both adults P1 and P3, and unaffected family members did not carry the variant. This variant was not found in several public databases, including gnomAD v.2.1.1 (>125,000 individuals), DiscovEHR (>50,000 individuals), and Geno2MP (>18,000 individuals). It is important to note the c.1267C>T variant is observed twice in Geno2MP, but both are from our individual P7 because he had both ES and GS. The variant was also absent from ClinVar.

### Generating CRISPR-edited Huh7 cells carrying the c.1267C>T (p.Arg423*) variant

Given the clear N-glycan abnormalities seen in serum samples from all seven affected individuals, we next sought to analyze N-glycans from fibroblasts. HPLC analyses of N-glycans from two affected individuals (P6 and P7) did not reveal any meaningful changes when compared against three healthy control fibroblast lines (data not shown). This was not completely unexpected given the liver-specific phenotype seen in the seven affected individuals. We also attempted to replicate the biochemical phenotype by either transiently or stably expressing the mutant transporter in

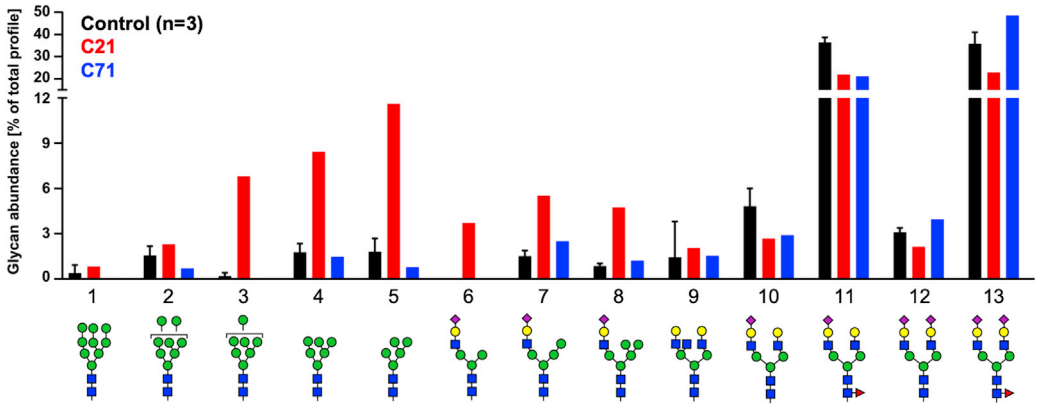


**Figure 3. Characterization of N-glycans from p.Arg423* base-edited Huh7 cells**
N-glycans released from secreted glycoproteins by PNGase F digestion showing the accumulation of both high mannose and hybrid type glycans in C21 with glycan abundances deduced from NSI-MSn measurements.

Huh7 or HEK293 cells. In both cell types, we failed to see measurable changes in the N-glycans (data not shown). However, it is critical to note we observed a significant rapid and progressive cell death from overexpressing either the wild-type or the mutant transporter by using either a strong (CMV) or a weaker (EF1) promoter. As an alternative approach, we generated iPSCs from P7 and carried out several successful experiments (see below). However, technical issues with the generation of iPSC-derived hepatocytes in sufficient quantities for experiments other than immunostaining led us to take a different approach.

Therefore, we CRISPR modified the hepatocarcinoma cell line, Huh7, and generated both heterozygous and homozygous c.1267C>T (p.Arg423*) clones. Genotyping showed several heterozygous clones with varying ratios of wild-type to mutant alleles. For example, Sanger sequencing showed clone C49 had a wild-type-to-mutant ratio of 40:60, while C71 was exactly 50:50, which matches affected individuals (Figure S4). We identified a single homozygous clone (C21) and multiple clones (C8, C9, and C10) that underwent treatment without producing an edit. These were used as Huh7 control lines because they were biochemically indistinguishable from the parental Huh7 cell line. In some cases, a silent variant c.1266C>T (p.G422G) also occurred (Figure S4).

### High mannose and hybrid type N-glycans in glycoproteins secreted from p.Arg423*-edited Huh7 cells

The hallmark of this disorder is the abnormal dramatic accumulation of high mannose and hybrid type N-glycans on liver-derived serum glycoproteins. We wanted to determine whether our CRISPR-edited Huh7 cells could replicate that N-glycan profile. Using NSI-MSn, we analyzed the N-glycans released from glycoproteins secreted by three isogenic controls (C8, C9, and C10) to clones carrying either a heterozygous (C71) or a homozygous (C21) c.1267C>T (p.Arg423*) variant in *SLC37A4*. C21 best replicated the N-glycan profile of the affected individuals, showing a substantial increase in the amount of high mannose (glycans 3–5) and hybrid type (glycans 6–8) N-glycans when compared with the three controls (Figure 3). C71 did not show a difference (Figure 3). HPLC analysis confirmed the observed N-glycan changes seen in C21 (Figure S5).

Glycan analysis of cell associated material from undifferentiated P7 iPSCs was identical to the control (K3), however, when P7 iPSCs were differentiated to hepatocytes, they replicated the accumulation of several, but not all, serum N-glycans seen in affected individuals (Figure S6). Specifically, hybrid type (glycans 10–12) N-glycans were the most significantly affected, while high/oligo mannose (glycans 1–5) were not.

### Mislocalized *SLC37A4*-encoded transporter in p.Arg423* -edited Huh7 cells

The c.1267C>T (p.Arg423*) in *SLC37A4* is predicted to delete the last seven amino acids from the cytoplasmic tail (423 - RVSKKAE - 429aa) (UniProt: O43826-1) (Figure 1C). This region includes a KKXX ER retrieval motif typically found in and required to maintain ER localization of resident proteins. However, the deleted region also has a possible Golgi retention sequence KXD/E motif (Figure 1C).[35,36] To better understand the consequences of losing these motifs, we used subcellular fractionation and confocal microscopy to compare wild-type or mutant transporter in our Huh7-edited cell lines.

Using a Nycodenz density gradient to fractionate subcellular organelles[29,30] of C9 control and C21 and C71, we clearly separate markers for ER (Calnexin) and *cis* Golgi (GM130) and found that neither the wild-type nor the mutant transporter was present in the Golgi fractions but enriched in the ER fractions (Figure 4A).

Next, we used high-resolution confocal microscopy to co-localize SLC37A4 with either the ER marker (anti-KDEL) or the Golgi marker (anti-GM130) in our mutant Huh7 lines. When compared with the two control Huh7 lines (C8 and C9), we did not see mislocalization of mutant SLC37A4 to the Golgi (Figure 4B). Instead, the majority

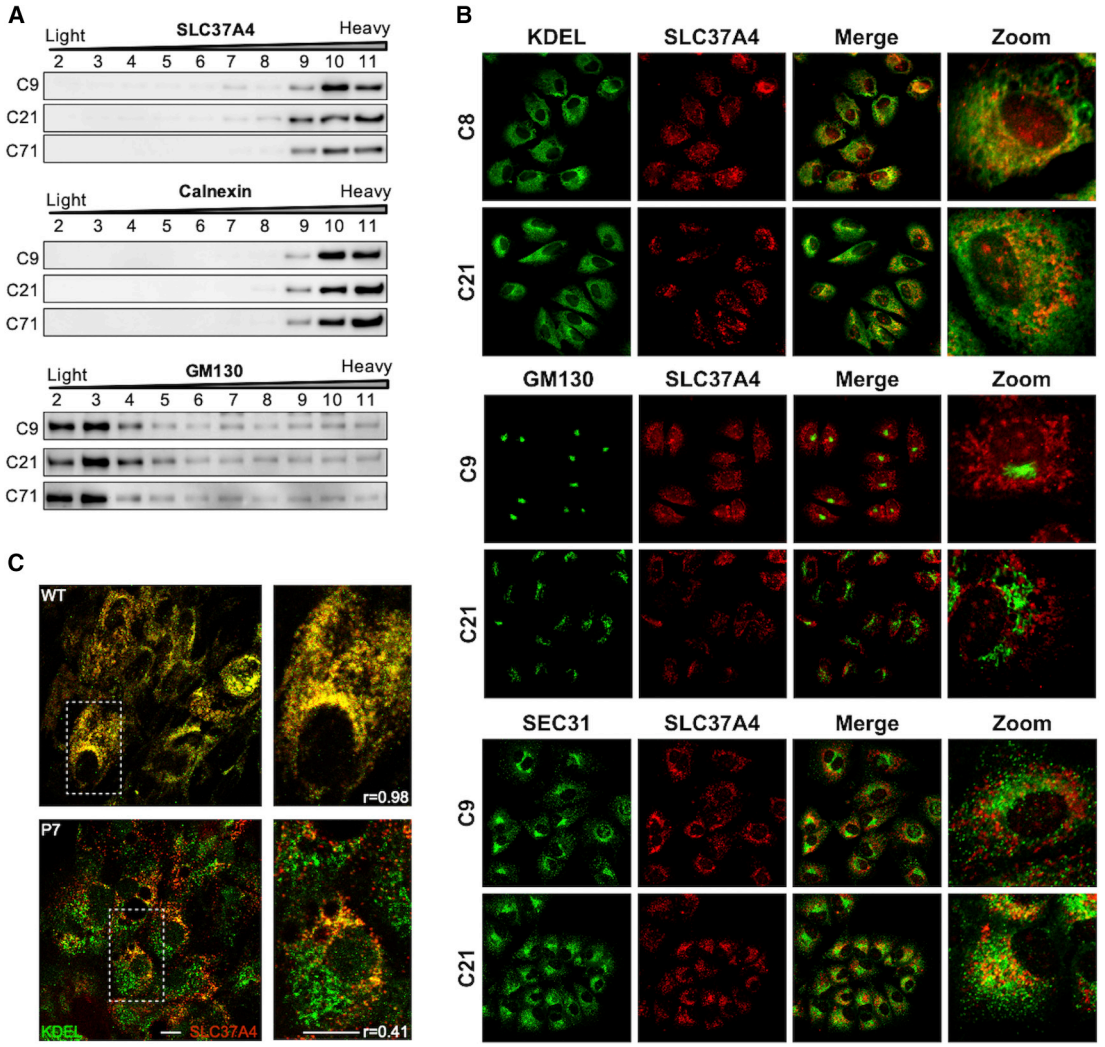


**Figure 4. Localization of mutant SLC37A4**

(A) Subcellular fractionations of extracts from control C9 and edited lines C21 and C71 showing SLC37A4 protein is absent from the GM130 Golgi-containing fractions, but with similar fractionation pattern as the ER marker, calnexin. Subcellular fractionations were performed with three biological replicates via the Nycodenz gradient method, and representative images are shown.

(B) Immunofluorescence staining of Huh7 control and edited cells showing localization of SLC37A4 with the ER marker, KDEL (upper panel), the Golgi marker, GM130 (middle panel), and the ER exit site marker, SEC31 (lower panel).

(C) Immunofluorescence staining for the ER marker, KDEL, and SLC37A4 in iPSC-derived hepatocytes from control and P7. Control (upper panel) showed strong colocalization (r = 0.98), while P7 (lower panel) showed reduced colocalization (r = 0.41).

remained in the ER-containing fractions. However, iPSC-derived differentiated hepatocytes showed an altered distribution of SLC37A4 within the ER. Analysis showed the KDEL-SLC37A4 overlap in control hepatocytes was substantial (R = 0.98), while in iPSC-derived P7 hepatocytes, this co-localization was far less pronounced (R = 0.41; R, Pearson correlation coefficient) (Figure 4C). It is not fully clear where this portion of mislocalized mutant transporter is residing within the early secretory pathway or whether the defect has caused alterations in the structure of the endoplasmic reticulum-Golgi intermediate compartment (ERGIC) compartment or mislocalization of the ER and ER exit site markers. In the Huh7 C21, we did see an increased colocalization of the ER exit site marker, SEC31, with SLC37A4, which was absent from controls (Figure 4B).

These data provide clear evidence that the mutant transporter is not localized to the Golgi, contradicting the claims of a previous report based on overexpression of the mutant transporter in HepG2 cells.[32] It is unclear where the mutant transporter resides, but it is most likely an undefined intermediate sub-compartment between the total ER and the *cis*-Golgi. The mutant transporter did not, however, colocalize with the ERGIC marker protein ERGIC-53 (Figure S7).

### Abnormal Golgi morphology and pH in p.Arg423* -edited Huh7 cells

While SLC37A4 was clearly not located in the Golgi, its redistribution correlated with a striking dose-dependent abnormal appearance in the Golgi morphology in both

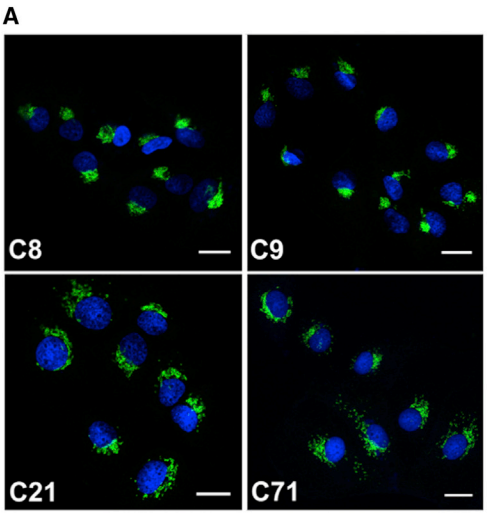


**Figure 5. Abnormal Golgi structure and function in p.Arg423* base-edited Huh7 cells**

(A) Immunofluorescence staining of Huh7 control (C8 and C9) and edited cells (C21 and C71) with the Golgi marker, GM130, showing abnormalities Golgi morphology/area. Scale bar represents 20 μm.

(B) Golgi area was quantified and then normalized to the area of the nucleus to provide a ratio showing both C21 (homozygous clone) and C71 (heterozygous clone) had significantly increased Golgi area. The effect is significantly more pronounced when both alleles are mutated as they are in C21. In three separate biological replicates, conducted within monthly intervals, each time with freshly thawed cells, n = 8 cells were analyzed, and the mean was taken. The graph represents an average of the means acquired over three different biological measurements. Total cells measured N = 24 over three biological replicates. Statistical significance *$p < 0.05$, **$p < 0.005$, ***$p < 0.001$, and ****$p < 0.0001$ was calculated via one-way ANOVA.

mutant clones (C21 and C71). Immunofluorescence staining with the Golgi-associated marker, GM130, showed a compact Golgi architecture in all three controls (C8, C9, and C10), while in mutant clones C21 and C71, the structure was reminiscent of Golgi fragmentation (Figure 5A). By measuring the ratio between the Golgi area versus the area of the nucleus, we were able to quantify this difference (Figure 5B). The abnormal distribution of *cis*-Golgi marker GM130 was also seen in the medial (Stx5 and Giantin) and *trans*-Golgi network (TGN46) markers that showed the same abnormal morphology (Figure S8). Because abnormal trafficking is a hallmark of many CDG Golgi defects, we examined the effects of brefeldin A (BFA)-induced retrograde transport in control and mutant cells but saw no apparent difference (Figure S9).

Because intra-Golgi pH is also critical for Golgi homeostasis, we also considered the possibility that an active SLC37A4 relocated to an inappropriate early compartment could indirectly increase the concentration of Glc-6P and/or Pi, leading to an altered intraluminal Golgi pH downstream. To test this, we transiently expressed a Golgi localized B4GALT1 protein fused to both a pH-sensitive eGFP and a pH-indifferent mCherry. Reduced Golgi pH lowers fluorescence of the modified eGFP, while the mCherry is unaffected (Figure 6A). Using this method, we determined the Golgi pH in two controls (C8 and C9) to be 6.23 and 6.21, respectively; C21 was approximately 5.51, 0.7 units lower than that of the controls (Figures 6A–6C), while the heterozygous C71 clone was intermediate at approximately 5.89. This method measures the entire Golgi and cannot discern the pH within each individual *cis*, medial, or *trans* compartment.[31]

### SLC37A4 transport activity in CRISPR-edited Huh7 cells

We previously mentioned that autosomal recessive loss-of-function variants in SLC37A4, which are primarily due to reduced Glc-6P transport activity, result in GSD-Ib. We show the p.Arg423* does not affect Glc-6P transport activity of SLC37A4 (Figure S10), which is consistent with previous findings showing that the last twelve amino acids of SLC37A4 are not required for protein stability or transport activity.[37] It also means that the mislocalized or redistributed mutants are fully capable of transporting and possibly accumulating Glc-6P.

## Discussion

We define a dominantly inherited metabolic disorder in seven individuals as a result of a p.Arg423* variant in *SLC37A4*, resulting in a liver-specific CDG characterized by altered serum protein N-glycosylation and a decreased series of coagulation proteins. These proteins include clotting factors (F2, F5, F9, and F11) and inhibitors (SERPINC1, PROS1, and PROC). Interestingly, three of our seven affected individuals also presented with cardiac abnormalities, which is also seen in G6PC3 deficiency.[38,39]

The p.Arg423* variant is predicted to delete a conserved C-terminal ER retrieval signal, which if removed, could result in mislocalization of a portion of the protein because affected individuals are heterozygous for the variant. It is known that varying-sized deletions within the C-terminal tail of SLC37A4 (as early as Arg418) do not impair its transport activity or stability, although localization was not addressed.[37] The C-terminal cytosolic tail of SLC37A4 contains a potential COP1-dependent Golgi retention signal KXD/E motif, suggesting possible inability to relocate a portion of the fully active protein to the Golgi. However, it should be noted that SLC37A4 has never been shown to be localized to the Golgi under physiological conditions.

Affected individuals who are compound heterozygous or homozygous for a p.Arg415* variant, which deletes the

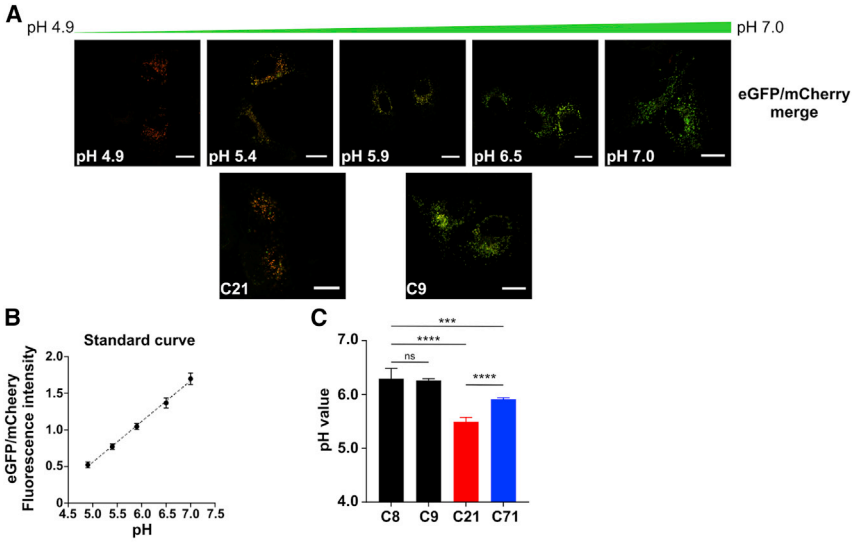


**Figure 6. Calibration and quantification of the Golgi pH in Huh7 control and edited cells**

(A) Calibration buffers were used to create a pH response curve for the GalT-mCherry-eGFP construct and allowed for the calculation of pH in Huh7 cells. Scale bar represents 20 μm.

(B) Standard curve using calibration buffers to determine estimated luminal pH values.

(C) Quantification of the Golgi luminal pH values in Huh7 controls (C8 and C9) and edited (C21, a homozygous clone, and C71, a heterozygous clone) cells showing acidification of the Golgi upon introduction of the c.1267C>T (p.Arg423*) mutation. The effect is significantly more pronounced when both alleles are mutated. Data were acquired in four (C8 and C71) or six (C9 and C21) biological replicates, conducted on different weeks, with cells freshly transfected with GalT-mCherry-eGFP construct. In each biological replicate, 10–15 cells were analyzed, and the mean was taken. The graph represents an average of the means acquired over the different biological measurements. Statistical significance *$p < 0.05$, **$p < 0.005$, ***$p < 0.001$, and ****$p < 0.0001$ was calculated via one-way ANOVA.

entire retrieval signal, have classical GSD-Ib. Biochemical studies show this variant reduces transport activity because of dramatically decreased transporter protein stability.[37] Glycosylation studies in one individual carrying the p.Arg415* variant were described as normal.[32] However, a lack of defective glycosylation could be due to the fact the p.Arg415* mutant is unstable and protein is lost. Therefore, the p.Arg415* mutant is unable to exert similar effects as the p.Arg423* variant, whose expression is not decreased (Figure S11).

The consequences of these differences in SLC37A4 protein expression highlight a key issue seen in both our study and the one reported by Marquardt et al.[32] In both studies, overexpression of either wild-type or mutant transporters was highly toxic, making interpretations from sick or dying cells unreliable.

We initially approached this problem and the lack of a measurable phenotype in fibroblasts by generating iPSCs from one individual (P7). While both control and P7 undifferentiated iPSCs showed no N-glycan abnormalities, we were able to show an abnormal N-glycan phenotype in hepatocytes derived from P7 (Figure S6). Because conversion of iPSCs to hepatocytes is lengthy and incomplete, we sought a more practical and reproducible approach to studying the c.1267C>T (p.Arg423*) variant in *SLC37A4* and opted to CRISPR-base edit Huh7 cells. We were able to generate several isogenic clones carrying variable ratios of wild-type to mutant transporter. This was very likely due to the presence of multiple gene copies of the transporter. These c.1267C>T (p.Arg423*) *SLC37A4*-modified Huh7 cell lines maintained stability of the mutant protein at comparable levels to controls (Figure S11). Fibroblasts from affected individuals also express similar levels of SLC37A4 protein to controls, but because they are not gluconeogenic cells, they do not exhibit an abnormal N-glycan phenotype. (Figure S11).

The CRISPR-edited Huh7 cells were found to have a gene dose-dependent abnormal Golgi morphology. There was a clear hierarchy of mutant SLC37A4 dose-dependent phenotypes: reduced Golgi pH → altered Golgi morphology → altered N-glycosylation of secreted and cellular proteins, possibly reflecting a cause-and-effect relationship.

We show mutant protein does not relocate to the Golgi, rather, it maintains activity and a portion of it localizes to an undefined region within the early secretory apparatus. Although several different approaches failed to show localization of the mutant transporter in the Golgi, we do show a portion localized with both an ER-marker (anti-KDEL) and a non-KDEL-containing compartment. This pattern was also seen in P7 hepatocyte-differentiated iPSCs (Figure 4C). We hypothesize the mutant transporter with its normal activity alters the localized environment within this undefined compartment and subsequently causes downstream changes via vesicular trafficking (Figure 7). These changes result in lower Golgi pH, which we hypothesize is sufficient to affect the activity or optimal organization of one or more Golgi-localized glycan maturation enzymes, also altering homeostasis and Golgi architecture (Figure 7). Glycosylation disorders impairing maintenance of luminal pH homeostasis have been reported (e.g., ATP6V0A2-CDG [MIM: 219200], ATP6V1A-CDG [MIM: 617403], ATP6V1E1-CDG [MIM: 617402], ATP6AP1-CDG [MIM: 300972], ATP6AP2-CDG [MIM: 301045], and SLC9A7-CDG [MIM: 301024]), and those disorders often display clear N-glycan and O-glycan defects involving galactosylation and sialylation but not the disturbance in earlier processing steps we observed.[40–44] While the cause of this pH change in our mutant lines remains unclear, we speculate that it is due to abnormal accumulation of Glc-6P or Glc+Pi, which would normally be transported back into the cytoplasm.

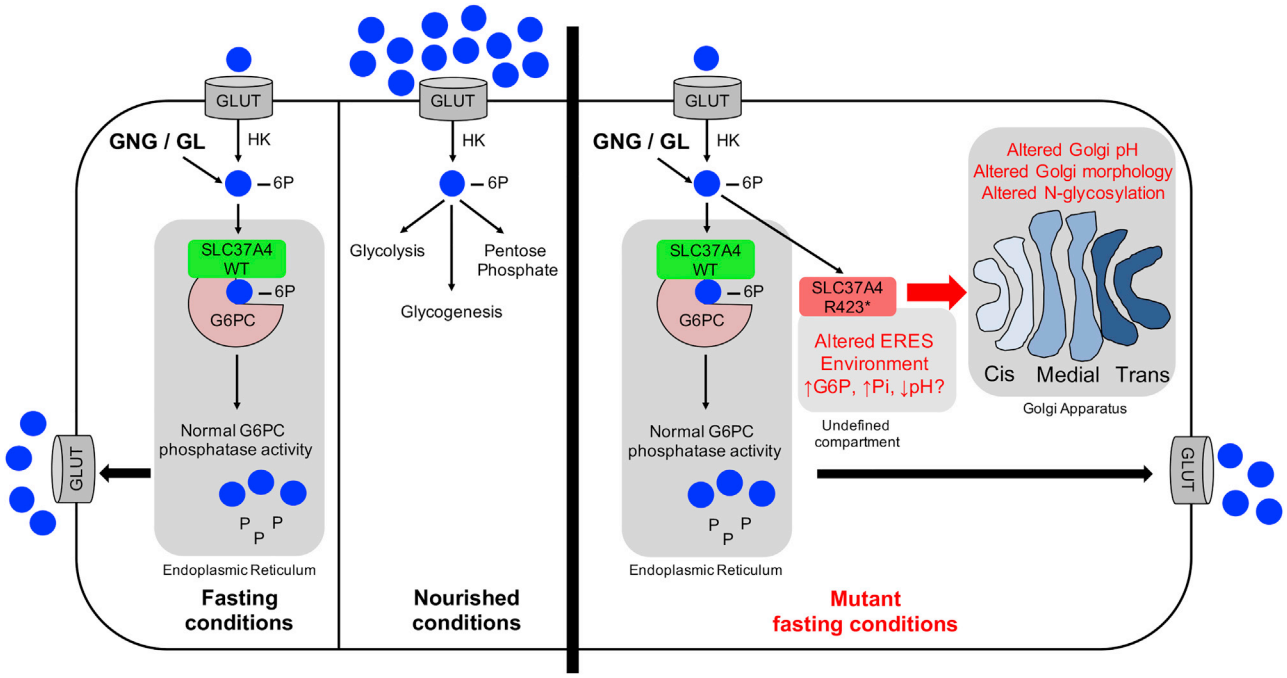


**Figure 7. Overview showing function of SLC37A4 in hepatocytes**
A schematic showing the function of wild-type SLC37A4 in hepatocytes during nourished or fasting conditions. Under nourished conditions, exogenous Glc provides ample Glc-6P for glycolysis, glycogenesis, and pentose phosphate pathways. Under fasting conditions, hepatocytes must generate Glc-6P from glycogenolysis (GL) and gluconeogenesis (GNG) for these pathways and also normalize plasma Glc. SLC37A4 imports Glc-6P into the ER and G6PC releases Pi+Glc so both can be returned to the cytoplasm and Glc to the circulation. Mutant SLC37A4 (p.Arg423*) is fully active and maintains normal glucose homeostasis under fasting conditions, but a portion of the active transporter becomes mislocalized to an undefined, spatially restricted pre-Golgi/post-ER compartment, possibly ERES. Glc-6P and/or Pi accumulates there, leading to a dose-dependent reduction of Golgi pH and Golgi architecture/homeostasis. Reduced pH is propagated in subsequent Golgi compartments, altering the activity and/or localization of multiple N- and O-glycan-modifying enzymes. Because Mn and Mg are critical co-factors for many of these reactions, reduced pH could affect their solubility and availability.

The dominantly inherited disorder presented here is characterized by liver dysfunction, coagulation deficiencies, and profound abnormalities in N-glycosylation of serum-specific proteins; the recessive form GSD-Ib only overlaps with the liver dysfunction. GSD-Ib does not present with the N-glycosylation deficiency seen in liver-specific factors, however neutrophils from affected individuals do show hypogalactosylation.[45] It is intriguing that both disorders do show hypogalactosylation, albeit in different tissue types, and suggests dysregulation of glucose homeostasis could be contributing to the hypogalactosylation. In GSD-Ib and G6PC3 deficiency, accumulation of 1,5-anhydroglucitol-6-phosphate significantly alters glucose homeostasis and causes the observed neutropenia and neutrophil dysfunction.[38,39]

Here, we present a dominantly inherited disorder of glycosylation due to a heterozygous c.1267C>T (p.Arg423*) variant in *SLC37A4*. Affected individuals present with a multifactorial coagulation defect characterized by abnormal serum glycoproteins specifically harboring high mannose and hybrid type N-glycans. Hepatoma cells base edited to carry the p.Arg423*variant recapitulate the N-glycan abnormality and additionally show a profoundly dysfunctional Golgi apparatus characterized by gene dosage-dependent hierarchy of reduced luminal pH, altered morphology, and disrupted homeostasis.

## Data and code availability

The accession number for the c.1267C>T (p.Arg423*) variant in *SLC37A4* is GenBank: NM_001164277.1. The UniProt ID is UniProt: O43826-1.

## Supplemental information

Supplemental information can be found online at https://doi.org/10.1016/j.ajhg.2021.04.013.

## Acknowledgments

We would like to thank all the families for their continued support and for providing valuable biological specimens and the SBP Medical Discovery Institute FACS core. This work was supported by The Rocket Fund and R01DK99551 (H.H.F.) and the European Union's Horizon 2020 research and innovation program under the ERA-NET cofund action no. 643578 (A.B., N.S., S.V.B., and T.D.). We thank Koen Galenkamp for providing technical assistance, plasmids, and reagents for pH measurements; Kazuhiro Aoki and Mayumi Ishihara for assistance with N-glycan analysis and annotation; and Jamie Smolin for her assistance. Exome sequencing for P1, P3, P4, and P5 was supported by a grant from Fondation Maladies Rares (FMR) as part of the high-throughput sequencing and rare diseases 2016 program WES-20160717. This work was also supported by Commissariat à l'Energie Atomique et aux Energies Alternatives and the MetaboHUB infrastructure (ANR-11-INBS-0010) (F.F.).

## Declaration of interests

The authors declare no competing interests.

Received: February 4, 2021
Accepted: April 20, 2021
Published: May 7, 2021

## Web resources

Combined Annotation Dependent Depletion (CADD), https://cadd.gs.washington.edu/
DiscovEHR, http://www.discovehrshare.com/
GenBank, https://www.ncbi.nlm.nih.gov/genbank/
Geno2MP, https://geno2mp.gs.washington.edu/Geno2MP/#/
Genome Aggregation Database (gnomAD), https://gnomad.broadinstitute.org/
Online Mendelian Inheritance in Man (OMIM), https://www.omim.org/

## References

1. Freeze, H.H., Chong, J.X., Bamshad, M.J., and Ng, B.G. (2014). Solving glycosylation disorders: fundamental approaches reveal complicated pathways. Am. J. Hum. Genet. *94*, 161–175.
2. Francisco, R., Marques-da-Silva, D., Brasil, S., Pascoal, C., Dos Reis Ferreira, V., Morava, E., and Jaeken, J. (2019). The challenge of CDG diagnosis. Mol. Genet. Metab. *126*, 1–5.
3. Ferreira, C.R., Altassan, R., Marques-Da-Silva, D., Francisco, R., Jaeken, J., and Morava, E. (2018). Recognizable phenotypes in CDG. J. Inherit. Metab. Dis. *41*, 541–553.
4. Hamdan, F.F., Myers, C.T., Cossette, P., Lemay, P., Spiegelman, D., Laporte, A.D., Nassif, C., Diallo, O., Monlong, J., Cadieux-Dion, M., et al.; Deciphering Developmental Disorders Study (2017). High Rate of Recurrent De Novo Mutations in Developmental and Epileptic Encephalopathies. Am. J. Hum. Genet. *101*, 664–685.
5. Li, M., Cheng, R., Liang, J., Yan, H., Zhang, H., Yang, L., Li, C., Jiao, Q., Lu, Z., He, J., et al. (2013). Mutations in POFUT1, encoding protein O-fucosyltransferase 1, cause generalized Dowling-Degos disease. Am. J. Hum. Genet. *92*, 895–903.
6. Takeuchi, H., Wong, D., Schneider, M., Freeze, H.H., Takeuchi, M., Berardinelli, S.J., Ito, A., Lee, H., Nelson, S.F., and Haltiwanger, R.S. (2018). Variant in human POFUT1 reduces enzymatic activity and likely causes a recessive microcephaly, global developmental delay with cardiac and vascular features. Glycobiology *28*, 276–283.
7. Ferreira, C.R., Xia, Z.J., Clément, A., Parry, D.A., Davids, M., Taylan, F., Sharma, P., Turgeon, C.T., Blanco-Sánchez, B., Ng, B.G., et al.; Undiagnosed Diseases Network; and Scottish Genome Partnership (2018). A Recurrent De Novo Heterozygous COG4 Substitution Leads to Saul-Wilson Syndrome, Disrupted Vesicular Trafficking, and Altered Proteoglycan Glycosylation. Am. J. Hum. Genet. *103*, 553–567.
8. Reynders, E., Foulquier, F., Leão Teles, E., Quelhas, D., Morelle, W., Rabouille, C., Annaert, W., and Matthijs, G. (2009). Golgi function and dysfunction in the first COG4-deficient CDG type II patient. Hum. Mol. Genet. *18*, 3244–3256.
9. Veiga-da-Cunha, M., Gerin, I., Chen, Y.T., de Barsy, T., de Lonlay, P., Dionisi-Vici, C., Fenske, C.D., Lee, P.J., Leonard, J.V., Maire, I., et al. (1998). A gene on chromosome 11q23 coding for a putative glucose- 6-phosphate translocase is mutated in glycogen-storage disease types Ib and Ic. Am. J. Hum. Genet. *63*, 976–983.
10. Chou, J.Y., Jun, H.S., and Mansfield, B.C. (2010). Glycogen storage disease type I and G6Pase-β deficiency: etiology and therapy. Nat. Rev. Endocrinol. *6*, 676–688.
11. Chou, J.Y., and Mansfield, B.C. (2014). The SLC37 family of sugar-phosphate/phosphate exchangers. Curr. Top. Membr. *73*, 357–382.
12. Hewitt, K.N., Walker, E.A., and Stewart, P.M. (2005). Minireview: hexose-6-phosphate dehydrogenase and redox control of 11beta-hydroxysteroid dehydrogenase type 1 activity. Endocrinology *146*, 2539–2543.
13. Hiraiwa, H., Pan, C.J., Lin, B., Moses, S.W., and Chou, J.Y. (1999). Inactivation of the glucose 6-phosphate transporter causes glycogen storage disease type 1b. J. Biol. Chem. *274*, 5532–5536.
14. Burchell, A., Jung, R.T., Lang, C.C., Bennet, W., and Shepherd, A.N. (1987). Diagnosis of type 1a and type 1c glycogen storage diseases in adults. Lancet *1*, 1059–1062.
15. Lei, K.J., Chen, Y.T., Chen, H., Wong, L.J., Liu, J.L., McConkie-Rosell, A., Van Hove, J.L., Ou, H.C., Yeh, N.J., Pan, L.Y., et al. (1995). Genetic basis of glycogen storage disease type 1a: prevalent mutations at the glucose-6-phosphatase locus. Am. J. Hum. Genet. *57*, 766–771.
16. Boztug, K., Appaswamy, G., Ashikov, A., Schäffer, A.A., Salzer, U., Diestelhorst, J., Germeshausen, M., Brandes, G., Lee-Gossler, J., Noyan, F., et al. (2009). A syndrome with congenital neutropenia and mutations in G6PC3. N. Engl. J. Med. *360*, 32–43.
17. Banka, S., Newman, W.G., Ozgül, R.K., and Dursun, A. (2010). Mutations in the G6PC3 gene cause Dursun syndrome. Am. J. Med. Genet. A. *152A*, 2609–2611.
18. Draper, N., Walker, E.A., Bujalska, I.J., Tomlinson, J.W., Chalder, S.M., Arlt, W., Lavery, G.G., Bedendo, O., Ray, D.W., Laing, I., et al. (2003). Mutations in the genes encoding 11beta-hydroxysteroid dehydrogenase type 1 and hexose-6-phosphate dehydrogenase interact to cause cortisone reductase deficiency. Nat. Genet. *34*, 434–439.
19. Si-Tayeb, K., Noto, F.K., Nagaoka, M., Li, J., Battle, M.A., Duris, C., North, P.E., Dalton, S., and Duncan, S.A. (2010). Highly efficient generation of human hepatocyte-like cells from induced pluripotent stem cells. Hepatology *51*, 297–305.
20. Colunga, T., Hayworth, M., Kress, S., Reynolds, D.M., Chen, L., Nazor, K.L., Baur, J., Singh, A.M., Loring, J.F., Metzger, M., et al. (2019). Human Pluripotent Stem Cell-Derived Multipotent Vascular Progenitors of the Mesothelium Lineage Have Utility in Tissue Engineering and Repair. Cell Rep. *26*, 2566–2579.e10.
21. Singh, A.M., Zhang, L., Avery, J., Yin, A., Du, Y., Wang, H., Li, Z., Fu, H., Yin, H., and Dalton, S. (2020). Human beige adipocytes for drug discovery and cell therapy in metabolic diseases. Nat. Commun. *11*, 2758.
22. Carchon, H.A., Chevigné, R., Falmagne, J.B., and Jaeken, J. (2004). Diagnosis of congenital disorders of glycosylation by capillary zone electrophoresis of serum transferrin. Clin. Chem. *50*, 101–111.
23. Lacey, J.M., Bergen, H.R., Magera, M.J., Naylor, S., and O'Brien, J.F. (2001). Rapid determination of transferrin isoforms by immunoaffinity liquid chromatography and electrospray mass spectrometry. Clin. Chem. *47*, 513–518.
24. Bengtson, P., Ng, B.G., Jaeken, J., Matthijs, G., Freeze, H.H., and Eklund, E.A. (2016). Serum transferrin carrying the xeno-tetrasaccharide NeuAc-Gal-GlcNAc2 is a biomarker of ALG1-CDG. J. Inherit. Metab. Dis. *39*, 107–114.

25. Yen-Nicolaÿ, S., Boursier, C., Rio, M., Lefeber, D.J., Pilon, A., Seta, N., and Bruneel, A. (2015). MALDI-TOF MS applied to apoC-III glycoforms of patients with congenital disorders affecting O-glycosylation. Comparison with two-dimensional electrophoresis. Proteomics Clin. Appl. *9*, 787–793.
26. Bruneel, A., Cholet, S., Drouin-Garraud, V., Jacquemont, M.L., Cano, A., Mégarbané, A., Ruel, C., Cheillan, D., Dupré, T., Vuillaumier-Barrot, S., et al. (2018). Complementarity of electrophoretic, mass spectrometric, and gene sequencing techniques for the diagnosis and characterization of congenital disorders of glycosylation. Electrophoresis *39*, 3123–3132.
27. Mehta, N., Porterfield, M., Struwe, W.B., Heiss, C., Azadi, P., Rudd, P.M., Tiemeyer, M., and Aoki, K. (2016). Mass Spectrometric Quantification of N-Linked Glycans by Reference to Exogenous Standards. J. Proteome Res. *15*, 2969–2980.
28. Keser, T., Pavić, T., Lauc, G., and Gornik, O. (2018). Comparison of 2-Aminobenzamide, Procainamide and *Rapi*Fluor-MS as Derivatizing Agents for High-Throughput HILIC-UPLC-FLR-MS N-glycan Analysis. Front Chem. *6*, 324.
29. Puglielli, L., Konopka, G., Pack-Chung, E., Ingano, L.A., Berezovska, O., Hyman, B.T., Chang, T.Y., Tanzi, R.E., and Kovacs, D.M. (2001). Acyl-coenzyme A: cholesterol acyltransferase modulates the generation of the amyloid beta-peptide. Nat. Cell Biol. *3*, 905–912.
30. Ko, M.H., and Puglielli, L. (2009). Two endoplasmic reticulum (ER)/ER Golgi intermediate compartment-based lysine acetyltransferases post-translationally regulate BACE1 levels. J. Biol. Chem. *284*, 2482–2492.
31. Galenkamp, K.M.O., Sosicka, P., Jung, M., Recouvreux, M.V., Zhang, Y., Moldenhauer, M.R., Brandi, G., Freeze, H.H., and Commisso, C. (2020). Golgi Acidification by NHE7 Regulates Cytosolic pH Homeostasis in Pancreatic Cancer Cells. Cancer Discov. *10*, 822–835.
32. Marquardt, T., Bzduch, V., Hogrebe, M., Rust, S., Reunert, J., Grüneberg, M., Park, J., Callewaert, N., Lachmann, R., Wada, Y., and Engel, T. (2020). SLC37A4-CDG: Mislocalization of the glucose-6-phosphate transporter to the Golgi causes a new congenital disorder of glycosylation. Mol. Genet. Metab. Rep. *25*, 100636.
33. Wilson, M.P., Quelhas, D., Leão-Teles, E., Sturiale, L., Rymen, D., Keldermans, L., Race, V., Souche, E., Rodrigues, E., Campos, T., et al. (2021). SLC37A4-CDG: Second patient. JIMD Rep. *58*, 122–128. https://doi.org/10.1002/jmd2.12195.
34. Crispin, M., Chang, V.T., Harvey, D.J., Dwek, R.A., Evans, E.J., Stuart, D.I., Jones, E.Y., Lord, J.M., Spooner, R.A., and Davis, S.J. (2009). A human embryonic kidney 293T cell line mutated at the Golgi alpha-mannosidase II locus. J. Biol. Chem. *284*, 21684–21695.
35. Gao, C., Cai, Y., Wang, Y., Kang, B.H., Aniento, F., Robinson, D.G., and Jiang, L. (2014). Retention mechanisms for ER and Golgi membrane proteins. Trends Plant Sci. *19*, 508–515.
36. Jackson, L.P., Lewis, M., Kent, H.M., Edeling, M.A., Evans, P.R., Duden, R., and Owen, D.J. (2012). Molecular basis for recognition of dilysine trafficking motifs by COPI. Dev. Cell *23*, 1255–1262.
37. Chen, L.Y., Lin, B., Pan, C.J., Hiraiwa, H., and Chou, J.Y. (2000). Structural requirements for the stability and microsomal transport activity of the human glucose 6-phosphate transporter. J. Biol. Chem. *275*, 34280–34286.
38. Veiga-da-Cunha, M., Chevalier, N., Stephenne, X., Defour, J.P., Paczia, N., Ferster, A., Achouri, Y., Dewulf, J.P., Linster, C.L., Bommer, G.T., and Van Schaftingen, E. (2019). Failure to eliminate a phosphorylated glucose analog leads to neutropenia in patients with G6PT and G6PC3 deficiency. Proc. Natl. Acad. Sci. USA *116*, 1241–1250.
39. Wortmann, S.B., Van Hove, J.L.K., Derks, T.G.J., Chevalier, N., Knight, V., Koller, A., Oussoren, E., Mayr, J.A., van Spronsen, F.J., Lagler, F.B., et al. (2020). Treating neutropenia and neutrophil dysfunction in glycogen storage disease type Ib with an SGLT2 inhibitor. Blood *136*, 1033–1043.
40. Kornak, U., Reynders, E., Dimopoulou, A., van Reeuwijk, J., Fischer, B., Rajab, A., Budde, B., Nürnberg, P., Foulquier, F., Lefeber, D., et al.; ARCL Debré-type Study Group (2008). Impaired glycosylation and cutis laxa caused by mutations in the vesicular H+-ATPase subunit ATP6V0A2. Nat. Genet. *40*, 32–34.
41. Van Damme, T., Gardeitchik, T., Mohamed, M., Guerrero-Castillo, S., Freisinger, P., Guillemyn, B., Kariminejad, A., Dalloyaux, D., van Kraaij, S., Lefeber, D.J., et al. (2017). Mutations in ATP6V1E1 or ATP6V1A Cause Autosomal-Recessive Cutis Laxa. Am. J. Hum. Genet. *100*, 216–227.
42. Jansen, E.J., Timal, S., Ryan, M., Ashikov, A., van Scherpenzeel, M., Graham, L.A., Mandel, H., Hoischen, A., Iancu, T.C., Raymond, K., et al. (2016). ATP6AP1 deficiency causes an immunodeficiency with hepatopathy, cognitive impairment and abnormal protein glycosylation. Nat. Commun. *7*, 11600.
43. Rujano, M.A., Cannata Serio, M., Panasyuk, G., Péanne, R., Reunert, J., Rymen, D., Hauser, V., Park, J.H., Freisinger, P., Souche, E., et al. (2017). Mutations in the X-linked *ATP6AP2* cause a glycosylation disorder with autophagic defects. J. Exp. Med. *214*, 3707–3729.
44. Khayat, W., Hackett, A., Shaw, M., Ilie, A., Dudding-Byth, T., Kalscheuer, V.M., Christie, L., Corbett, M.A., Juusola, J., Friend, K.L., et al. (2019). A recurrent missense variant in SLC9A7 causes nonsyndromic X-linked intellectual disability with alteration of Golgi acidification and aberrant glycosylation. Hum. Mol. Genet. *28*, 598–614.
45. Letkemann, R., Wittkowski, H., Antonopoulos, A., Podskabi, T., Haslam, S.M., Föll, D., Dell, A., and Marquardt, T. (2017). Partial correction of neutrophil dysfunction by oral galactose therapy in glycogen storage disease type Ib. Int. Immunopharmacol. *44*, 216–225.

**The American Journal of Human Genetics, Volume *108***

## Supplemental information

# A mutation in *SLC37A4* causes a dominantly inherited congenital disorder of glycosylation characterized by liver dysfunction

**Bobby G. Ng, Paulina Sosicka, François Fenaille, Annie Harroche, Sandrine Vuillaumier-Barrot, Mindy Porterfield, Zhi-Jie Xia, Shannon Wagner, Michael J. Bamshad, Marie-Christine Vergnes-Boiteux, Sophie Cholet, Stephen Dalton, Anne Dell, Thierry Dupré, Mathieu Fiore, Stuart M. Haslam, Yohann Huguenin, Tadahiro Kumagai, Michael Kulik, Katherine McGoogan, Caroline Michot, Deborah A. Nickerson, Tiffany Pascreau, Delphine Borgel, Kimiyo Raymond, Deepti Warad, University of Washington Center for Mendelian Genomics (UW-CMG), Heather Flanagan-Steet, Richard Steet, Michael Tiemeyer, Nathalie Seta, Arnaud Bruneel, and Hudson H. Freeze**

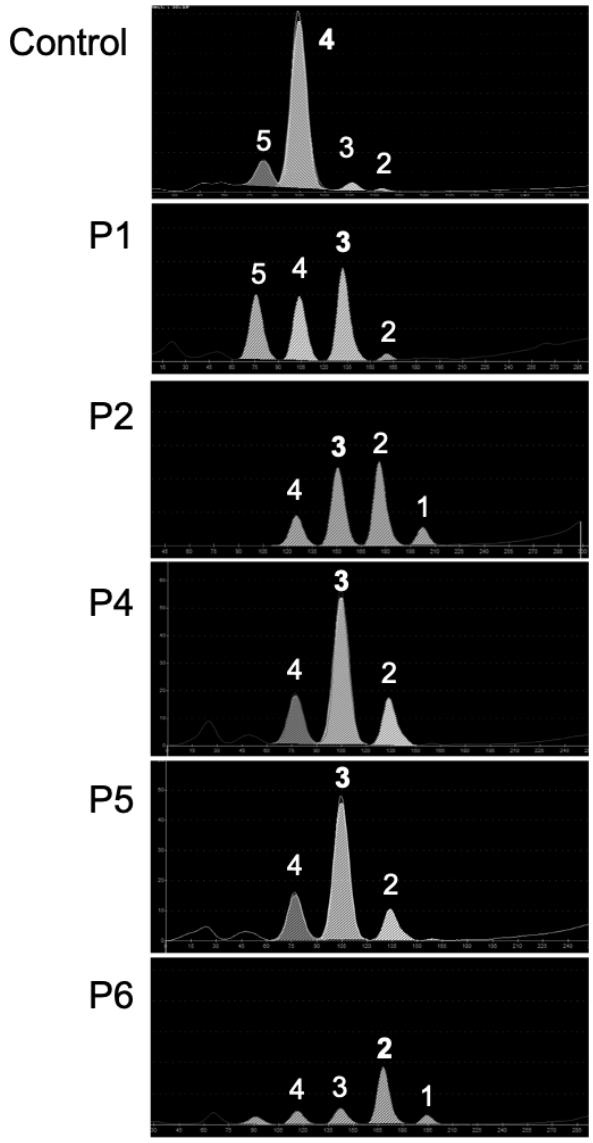


**Figure S1: Capillary zone electrophoresis of transferrin for Control, P1, P2, P4, P5, P6.** Glycosylated transferrin isoforms were separated by capillary zone electrophoresis with each peak labeled with the corresponding number of sialic acids. 0-Asiaolo, 1-Monosialo, 2-Disialo, 3-Trisialo, 4-Tetrasialo, 5-Pentasialo.

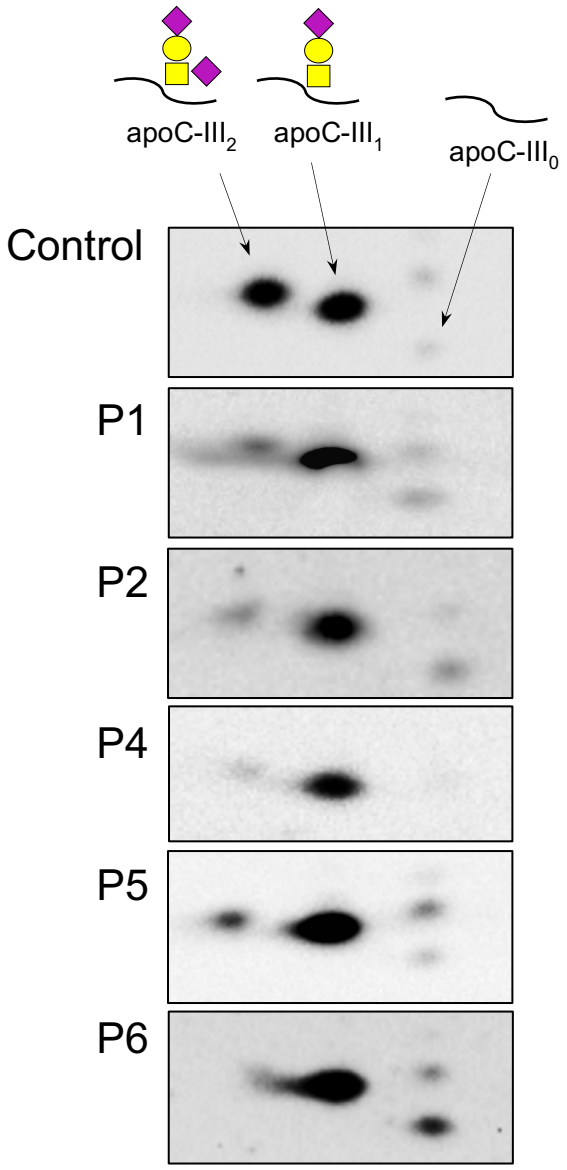


**Figure S2: 2-Dimensional gel electrophoresis of ApoCIII for Control, P1, P2, P4, P5, P6.** 2-DG electrophoresis of the serum O-linked glycoprotein, ApoCIII showing changes in the ratio of di-sialo ($ApoCIII_2$), mono-sialo ($ApoCIII_1$) and Asialo ($ApoCIII_0$).

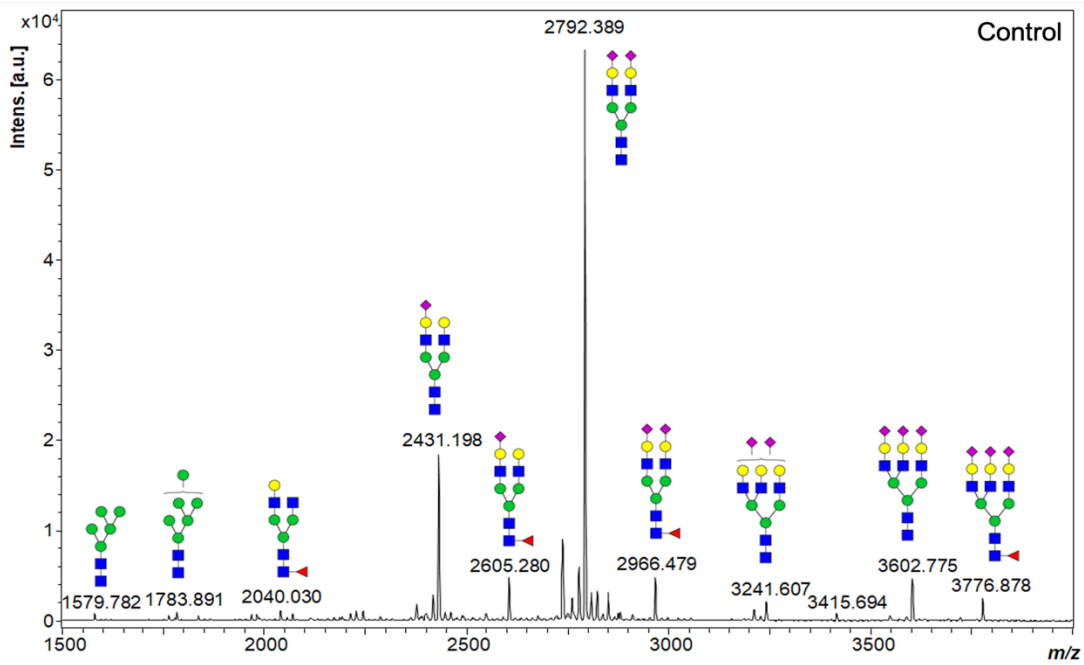
Control
x10⁴
Intens. [a.u.]
2792.389
2431.198
2605.280
2966.479
3241.607
3415.694
3602.775
3776.878
1579.782
1783.891
2040.030
m/z

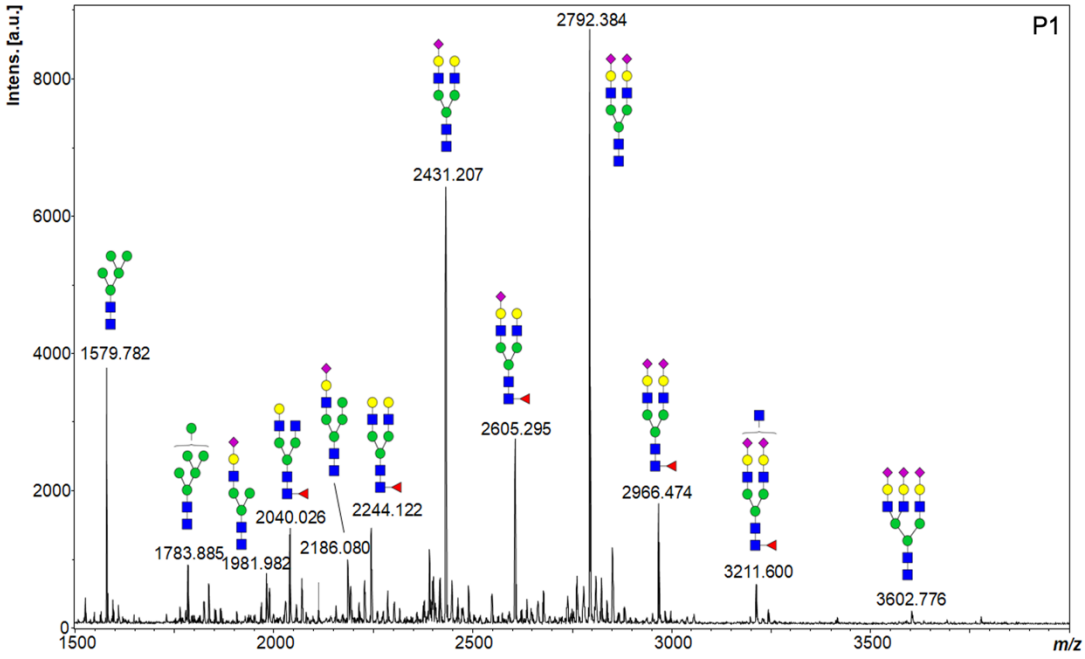
P1
Intens. [a.u.]
2792.384
2431.207
2605.295
2966.474
3211.600
3602.776
1579.782
1783.885
1981.982
2040.026
2186.080
2244.122
m/z

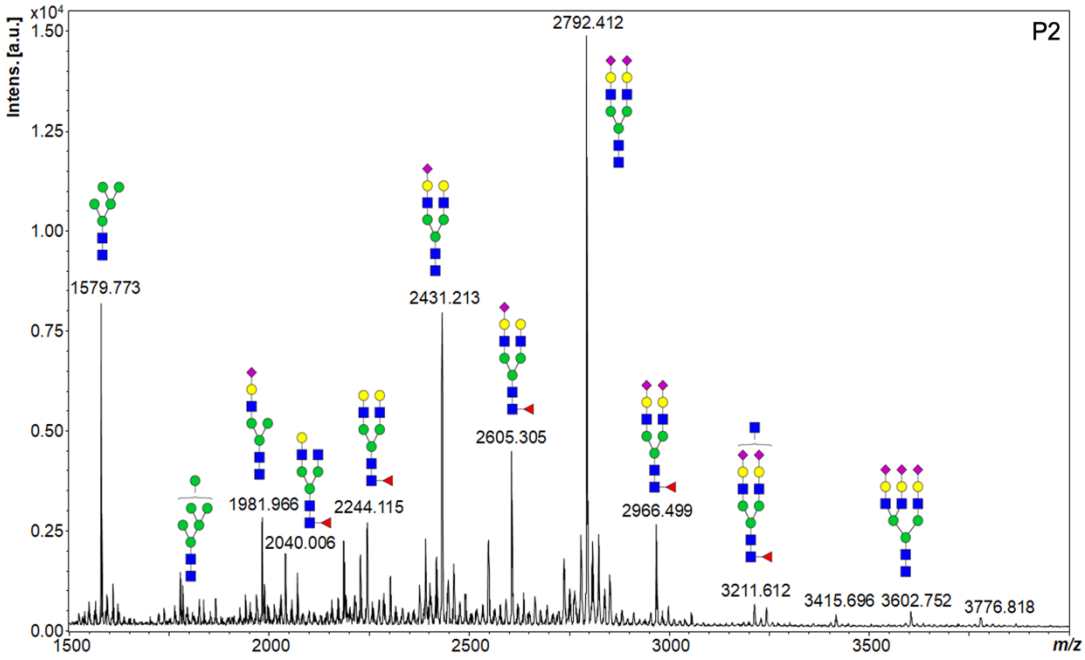
P2
Intens. [a.u.]
x10^4
1.50
1.25
1.00
0.75
0.50
0.25
0.00
1500
2000
2500
3000
3500
m/z
2792.412
1579.773
2431.213
2605.305
1981.966
2244.115
2040.006
2966.499
3211.612
3415.696
3602.752
3776.818

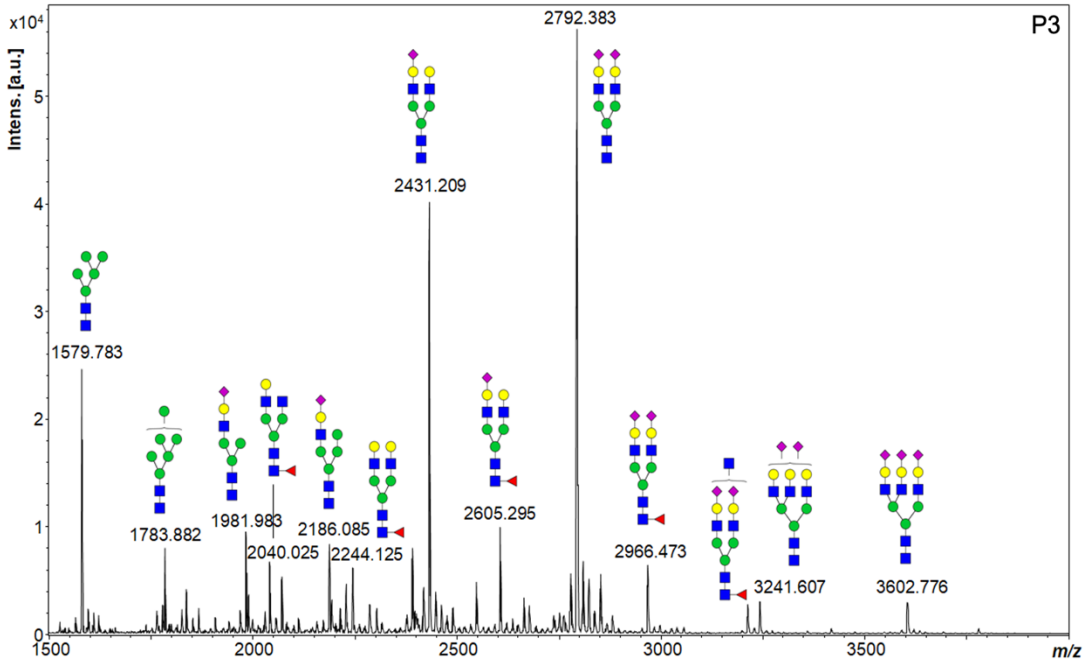
P3
Intens. [a.u.]
x10^4
5
4
3
2
1
0
1500
2000
2500
3000
3500
m/z
2792.383
2431.209
1579.783
1783.882
1981.983
2040.025
2186.085
2244.125
2605.295
2966.473
3241.607
3602.776

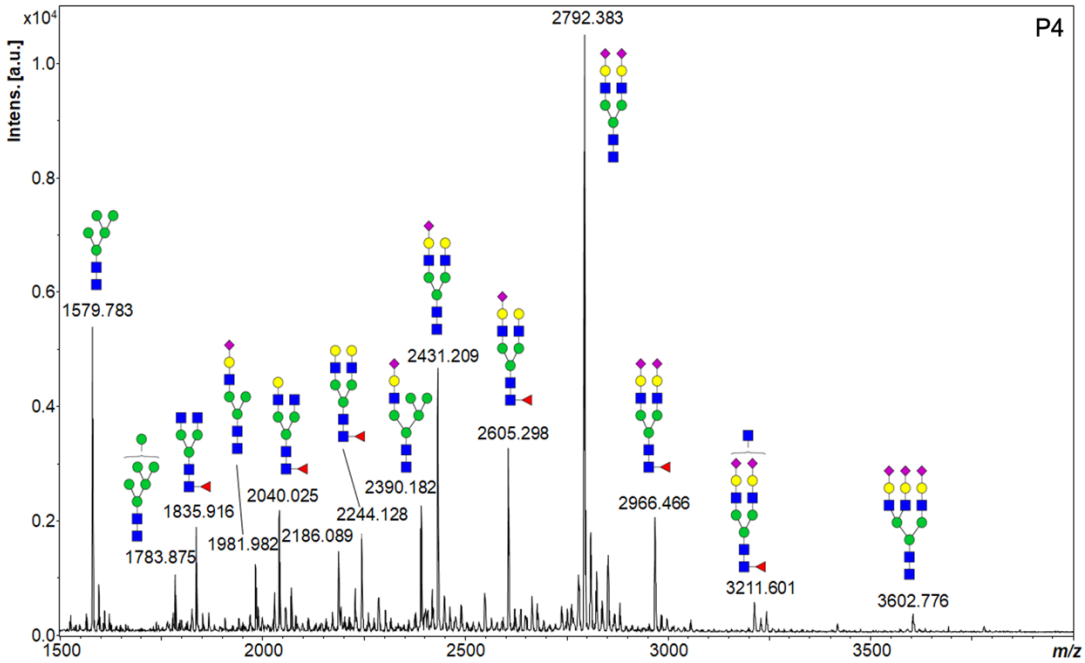
P4
x10^4
Intens. [a.u.]
1.0
0.8
0.6
0.4
0.2
0.0
1500
2000
2500
3000
3500
m/z
2792.383
1579.783
2431.209
2605.298
2966.466
3211.601
3602.776
1783.875
1835.916
1981.982
2040.025
2186.089
2244.128
2390.182

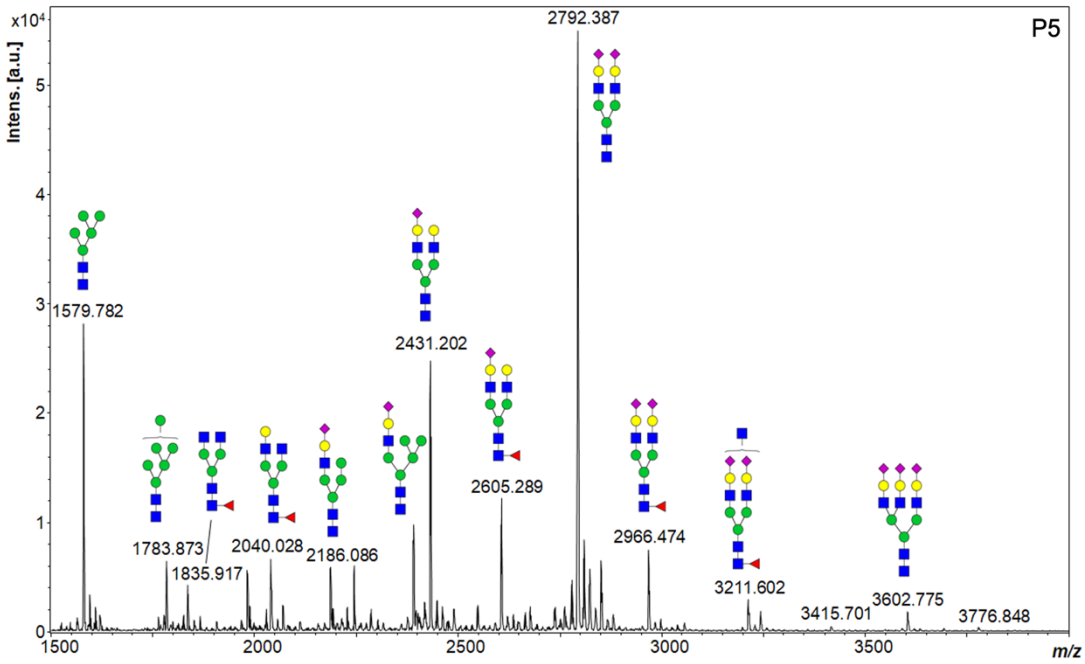
P5
x10^4
Intens. [a.u.]
5
4
3
2
1
0
1500
2000
2500
3000
3500
m/z
2792.387
1579.782
2431.202
2605.289
2966.474
3211.602
3602.775
3415.701
3776.848
1783.873
1835.917
2040.028
2186.086

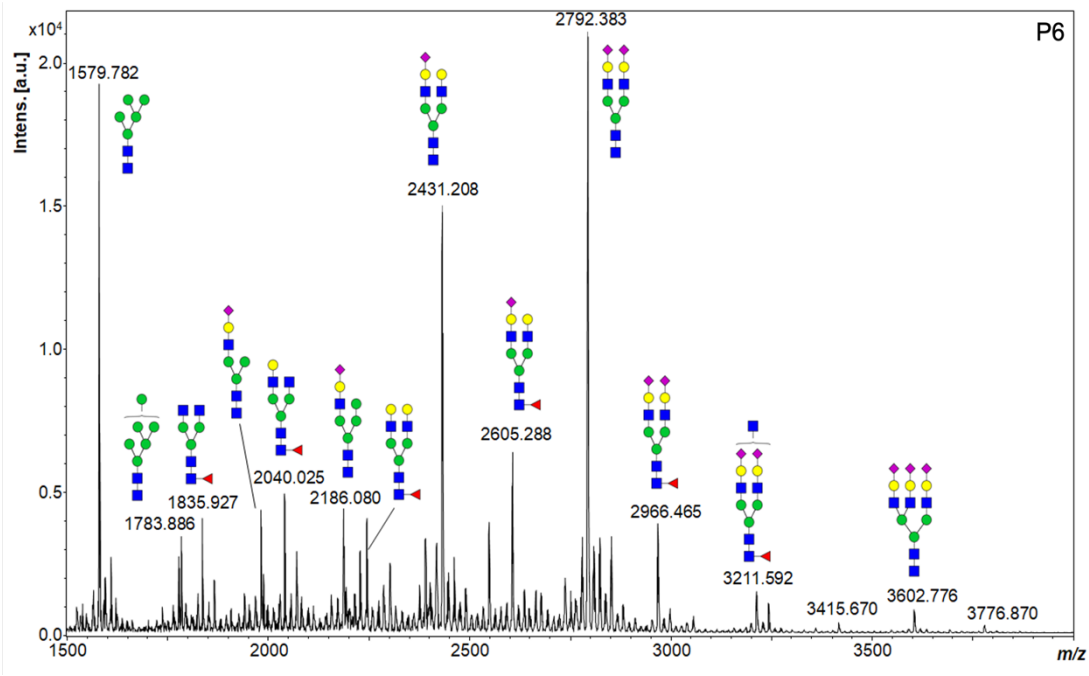
P6
x10^4
Intens. [a.u.]
2.0
1.5
1.0
0.5
0.0
1579.782
2792.383
2431.208
2605.288
2040.025
2186.080
1835.927
1783.886
2966.465
3211.592
3602.776
3415.670
3776.870
1500
2000
2500
3000
3500
m/z

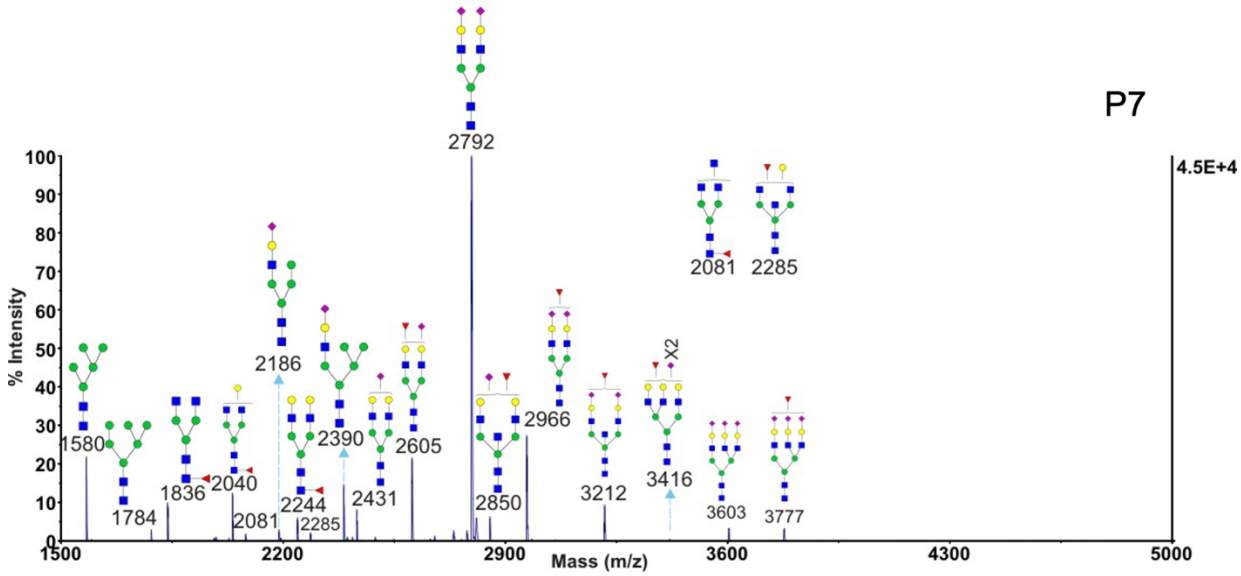
P7
2792
4.5E+4
% Intensity
100
90
80
70
60
50
40
30
20
10
0
2081
2285
2186
X2
1580
2966
2390
2605
1836
2040
3212
3416
1784
2244
2431
2850
3603
3777
2081
2285
1500
2200
2900
3600
4300
5000
Mass (m/z)

**Figure S3: Characterization of N-glycan abnormalities in serum from affected individuals.** MS spectra of N-glycans from serum glycoproteins for control and all seven affected unrelated individuals showing N-glycan abnormalities in serum. Specifically, the accumulation of multiple species of both high mannose (peaks 1579.8,1783.9m/z) and hybrid type N-glycans was observed (peaks 1981.9, 2186.1, 2390.2m/z).

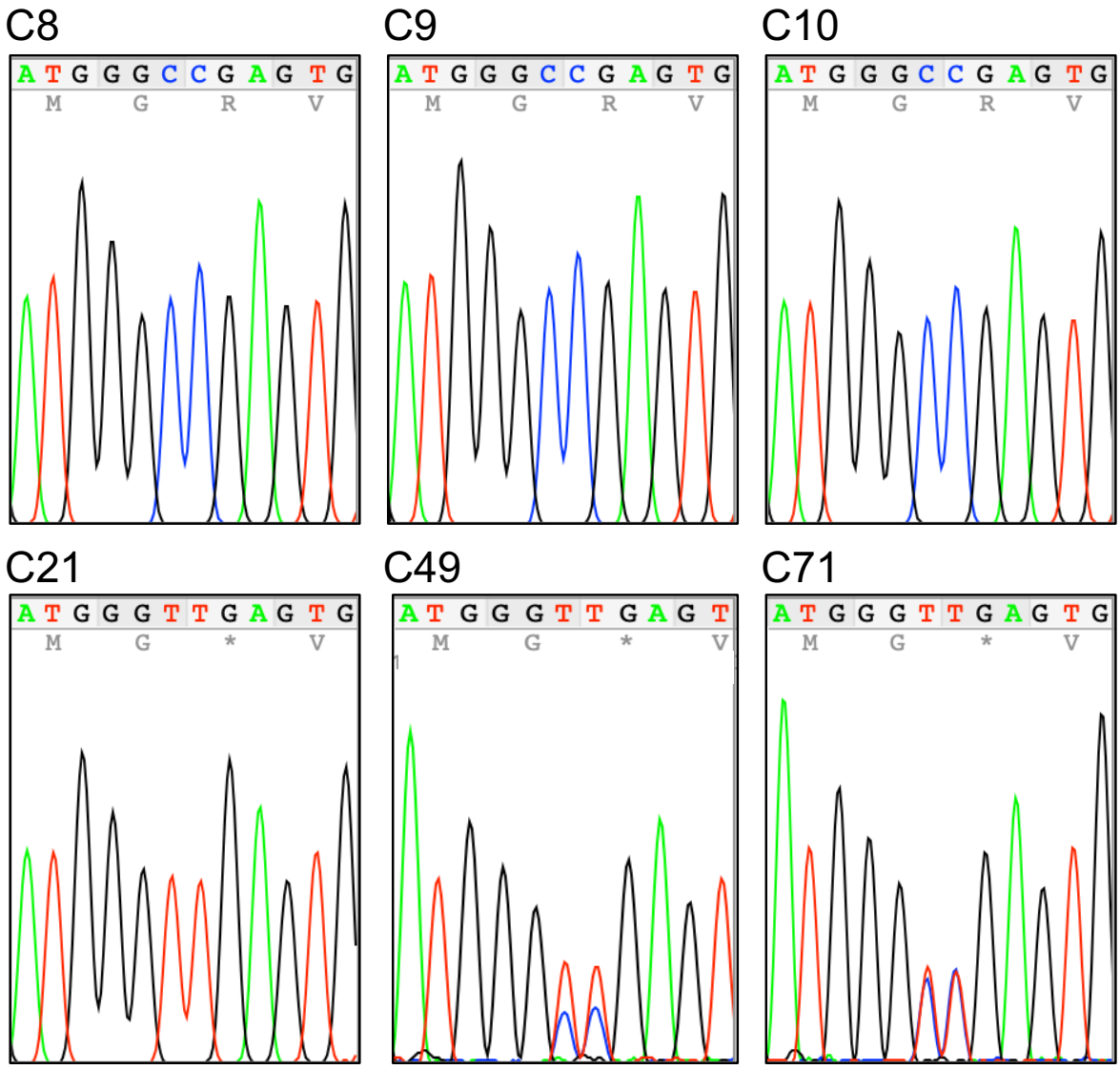


**Figure S4: Sanger sequencing of Huh7 base edited clones.** Sanger sequencing isogenic Huh7 base edited clones for the c.1267C>T [p.Arg423*] in *SLC37A4.* Clones C8, C9, C10 underwent the same editing process as C21, C49, C71 but no edit was performed.

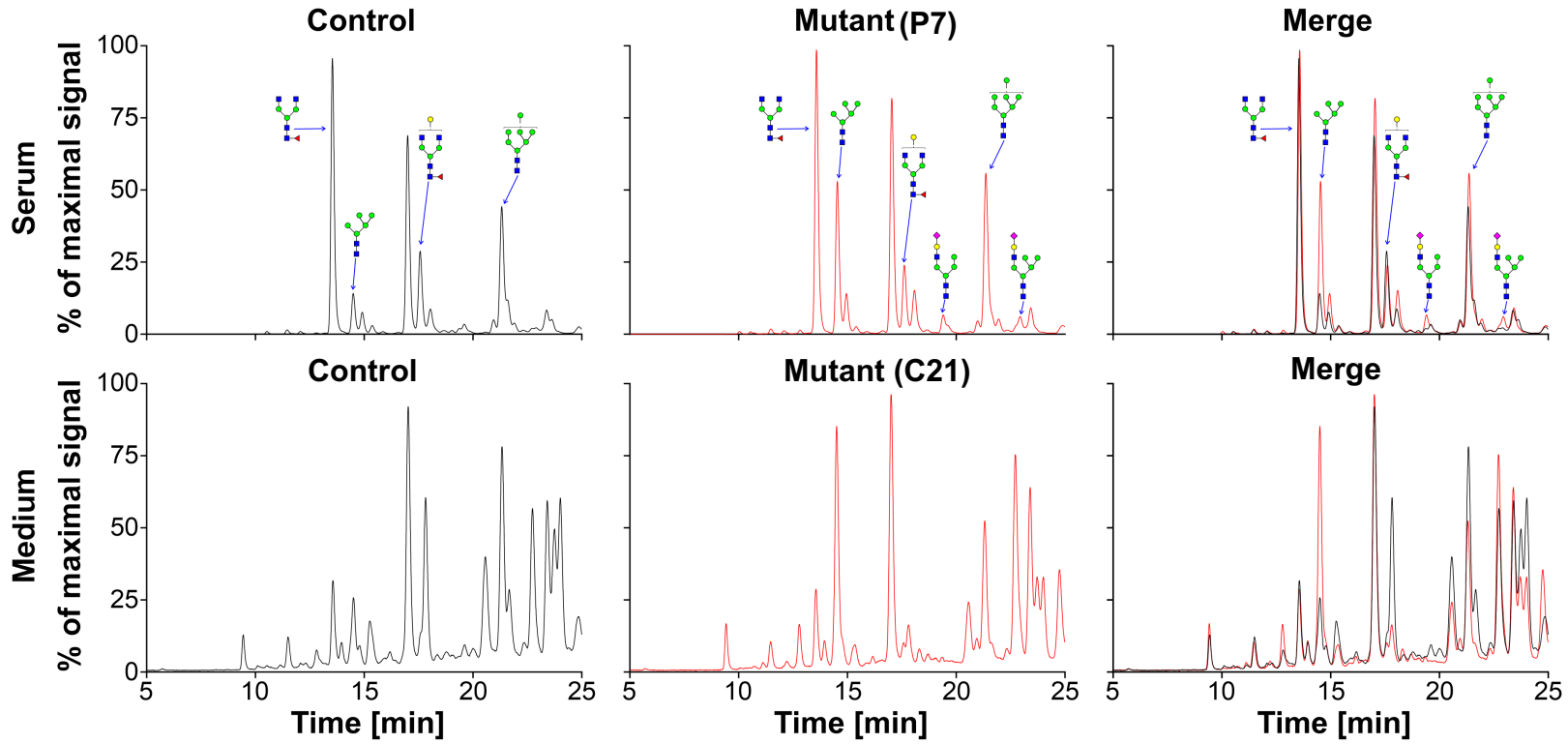


**Figure S5: HPLC analysis of N-glycans.** N-glycans were purified from Control and P7 serum (upper panel) as well as Huh7 Control and C21 medium (lower panel). Samples were run on HPLC and detected by fluorescence.

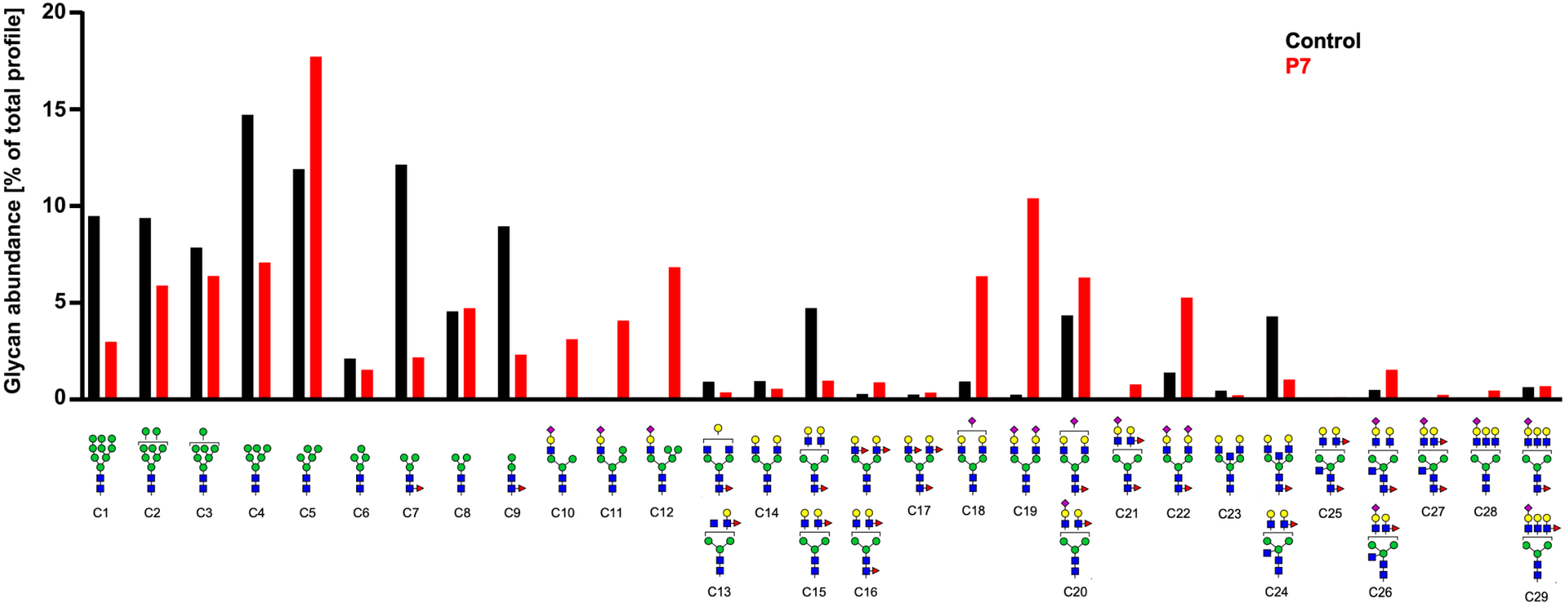
Glycan abundance [% of total profile]
20
15
10
5
0
Control
P7
C1
C2
C3
C4
C5
C6
C7
C8
C9
C10
C11
C12
C13
C14
C15
C16
C17
C18
C19
C20
C21
C22
C23
C24
C25
C26
C27
C28
C29

**Figure S6: Nanospray ionization mass spectrometry (NSI-MSn) analysis of N-glycans released from iPSC-derived hepatocytes.** Control and P7 iPSCs were differentiated to hepatocytes. N-glycans were released from total cell-associated proteins and analyzed after permethylation.

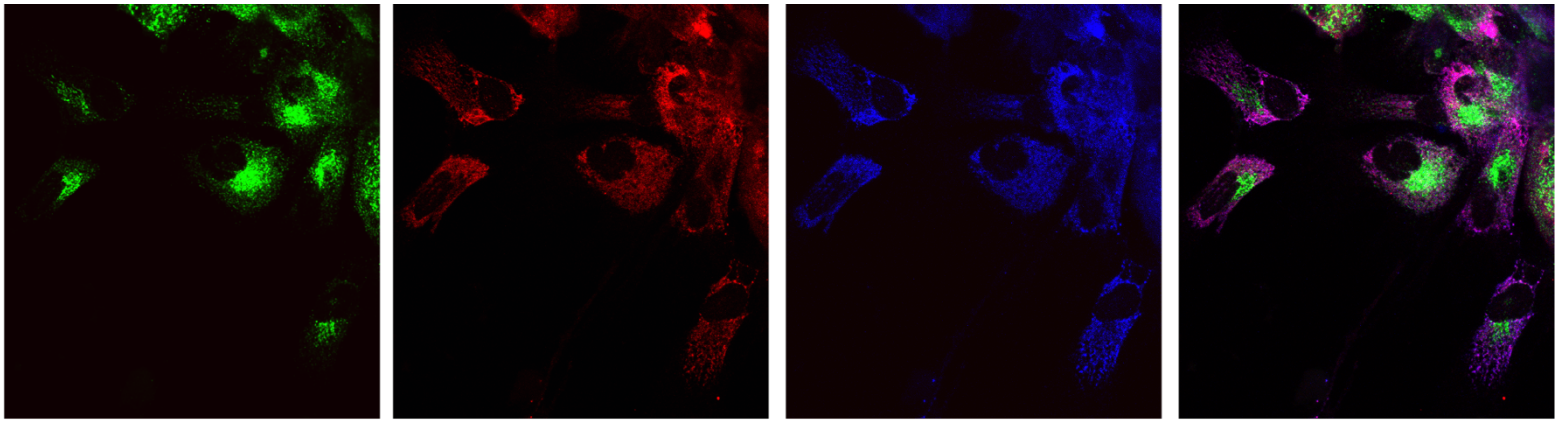


**Figure S7: ERGIC53 and SLC37A4 do not colocalize.** Immunofluorescence staining showing no colocalization of SLC37A4 with ERGIC53 in IPSC differentiated hepatocytes from P7.

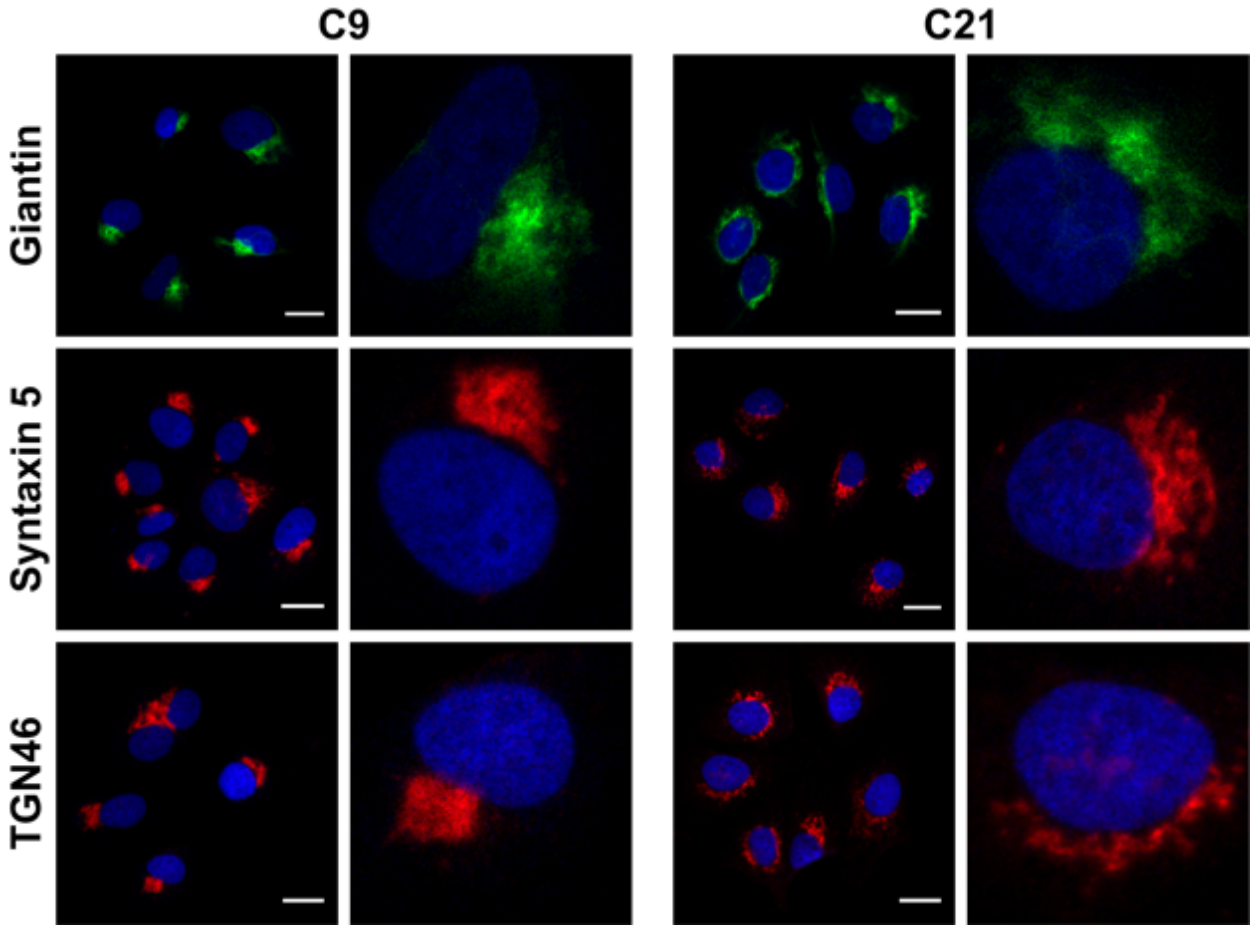


**Figure S8: Immunofluorescence for the Golgi morphology.** Multiple markers covering the three Golgi compartments were used to confirm abnormalities seen in the Golgi morphology. cis-Golgi/medial marker giantin, medial marker syntaxin 5 and trans marker Golgi network TGN46.

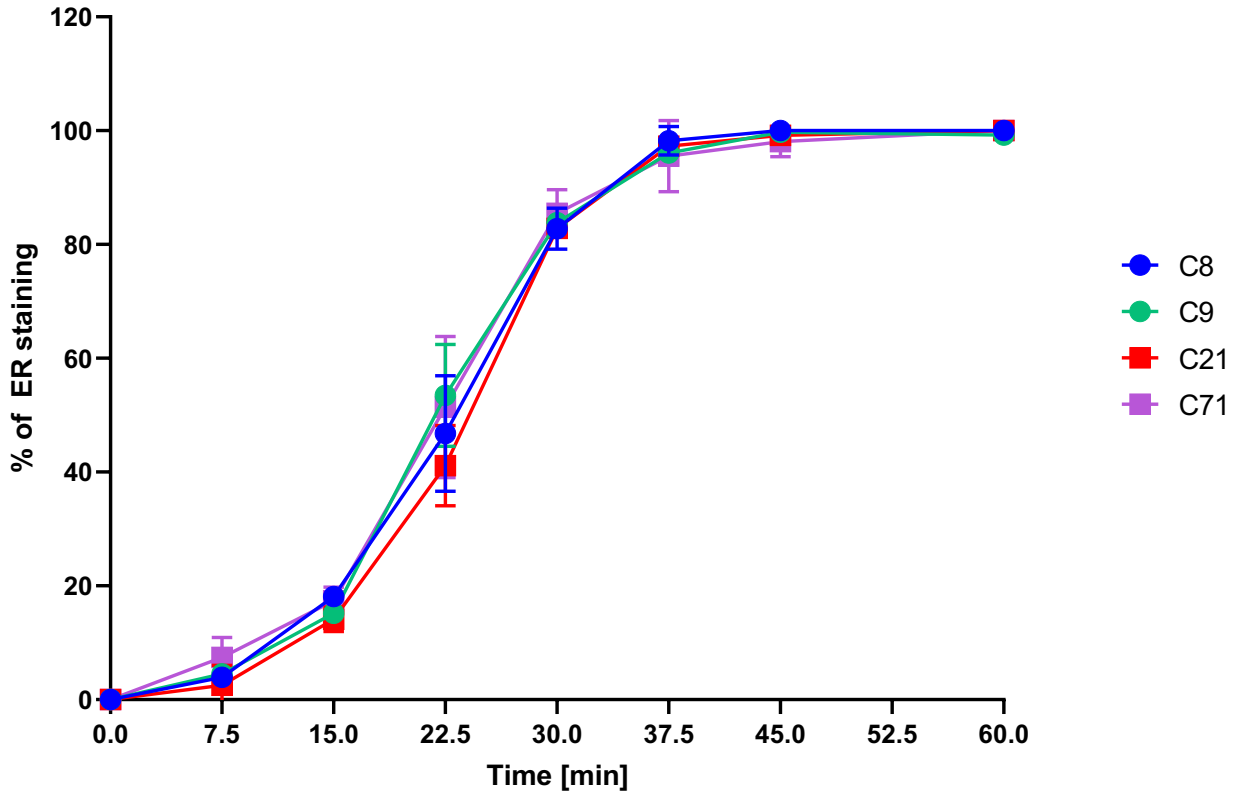


**Figure S9: Brefeldin A induced retrograde transport.**

Brefeldin A induced retrograde transport was assayed in each cell line and showed no difference in retrograde transport rate.

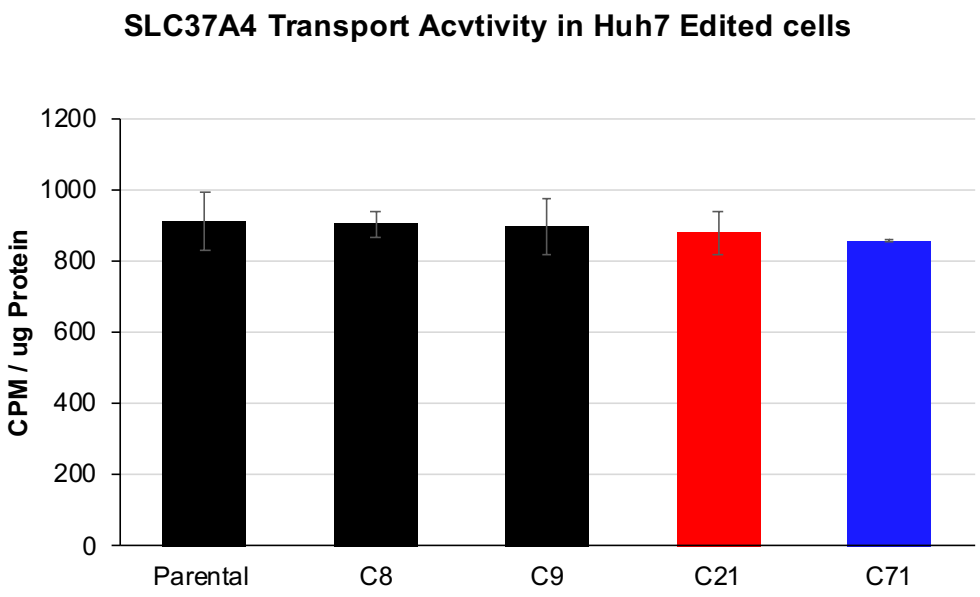


**Figure S10: SLC37A4 transport activity in CRISPR edited Huh7 cells.** SLC37A4 transport activity showing no difference in the ER specific uptake of $^{3}$H-Glc-6P into Huh7 control or edited cells.

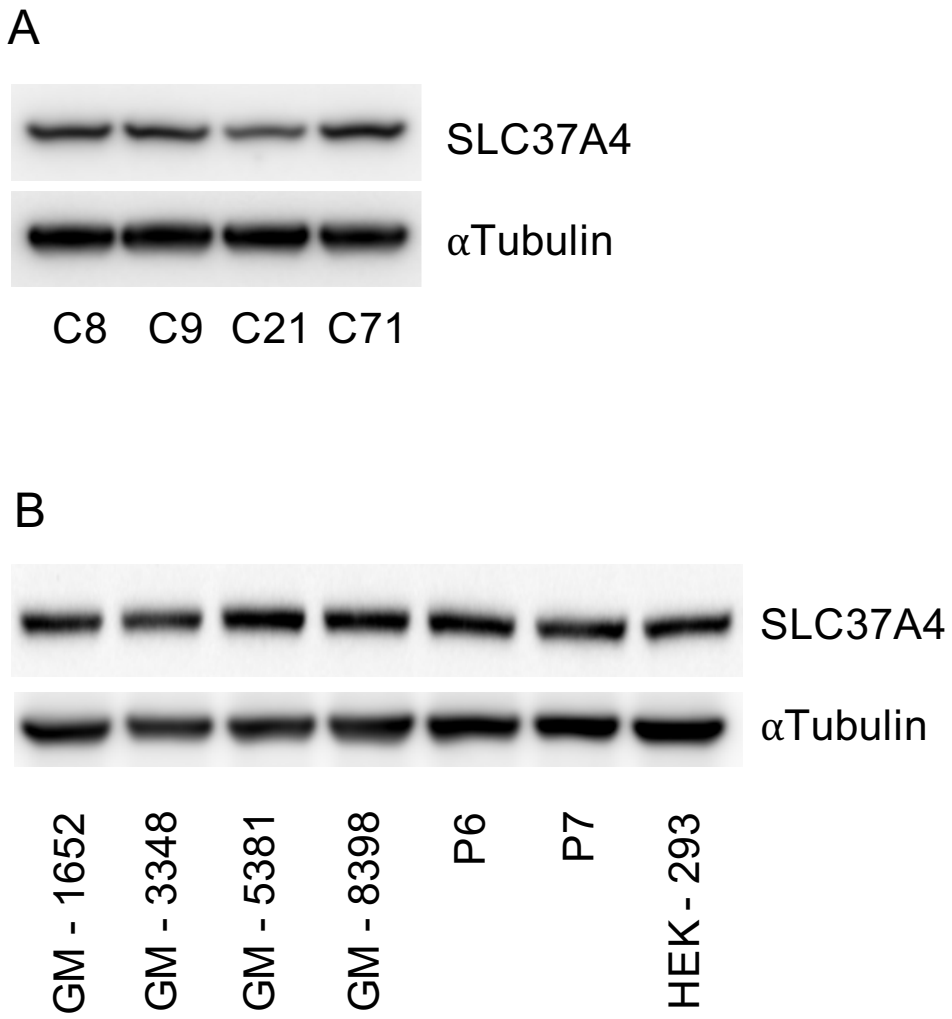


**Figure S11: SLC37A4 protein expression.** Western blot analysis of SLC37A4 expression in (A) Huh7 control (C8, C9) and edited (C21, C71) cells. (B) Expression of SLC37A4 in control GM – 1652, GM – 3348, GM – 5381 and P6, P7. Alpha tubulin was used to normalize protein levels.

**Table S1: List of primary and secondary antibodies used in immunofluorescence.**

| Antibody | Cat. Number | Source | Dilution | Company |
|---|---|---|---|---|
| anti-SLC37A4 | PA5-58599 | Rabbit | 1:100 | Life Technologies |
| anti-GM130 | 610822 | Mouse | 1:250 | BD Biosciences |
| anti-giantin Alexa Fluor 488 | 308701 | Rabbit | 1:250 | BioLegend |
| anti-syntaxin 5 | SC-365124 | Mouse | 1:100 | Santa Cruz Biotechnology Inc. |
| anti-TGN46 | GTX-74290 | Sheep | 1:100 | Genetex |
| anti-KDEL | ADI-SPA-827-D | Mouse | 1:100 | Enzo Life Sciences Inc. |
| anti-β4-GalT1 | HPA-010807-100uL | Rabbit | 1:100 | Sigma Aldrich |
| anti-Sec31A | 612350 | Mouse | 1:100 | BD Biosciences |
| anti-rabbit Alexa Fluor 405 | A31556 | Goat | 1:100 | Life Technologies |
| anti-rabbit Alexa Fluor 488 | AB150077 | Goat | 1:500 | Abcam |
| anti-rabbit Alexa Fluor 568 | A11011 | Goat | 1:250 | Life Technologies |
| anti-sheep Alexa Fluor 488 | AB150178 | Donkey | 1:250 | Abcam |
| anti-mouse Alexa Fluor 546 | A11003 | Goat | 1:250 | Life Technologies |